Colorado State University

ESSAYS ON RIVER MECHANICS

Presented by the Graduate Students
in CE 717 - River Mechanics (Spring, 1996)

Instructor: P.Y. Julien

April, 1996

CER95-96-PYJ-2

FOREWORD

I am very pleased to honor the work of the graduate students in the class CE-717 River Mechanics with this report of their technical papers. Each student worked on a particular aspect of river engineering in order to meet the following objectives:

1) familiarize with the recent literature and new methodologies not available in textbooks;
2) compare various methods (new versus old) and discuss the advancement of engineering technology on a given topic;
3) develop skills to point out the key elements of recent technological developments;
4) share interesting findings with the other students through an oral presentation and a written paper.

The requirements for this project were:

1) select a topic relevant to river mechanics and sediment transport;
2) conduct a literature review including papers published in the past five years;
3) compare new methods with those detailed in textbooks on either a theoretical basis or through comparison with an appropriate data set;
4) write a 12 page paper following the ASCE editorial standards (these papers are included herein);
5) summarize the analysis and discuss the major findings in a 20 minute oral presentation.

The reader will certainly agree with me that the objectives were met with great success. I am personally impressed with the overall quality of the reports presented and I can only compliment them all on their effort.

Pierre Y. Julien
Professor
Civil Engineering Department

TABLE OF CONTENTS

CE717 - Class Project

A Discussion of Overland Erosion Schemes

by

Billy E. Johnson

Spring 1996

ABSTRACT

Every sediment particle that passes a given stream cross section must satisfy the following two conditions (Einstein, 1964): 1.) It must have been eroded somewhere in the watershed above the cross section; and 2). It must be transported by the flow from the place of erosion to the cross section.

In this paper, I will describe three widely used overland erosion schemes, namely the USLE, the RUSLE, and the MUSLE. Finally, I will apply the MUSLE scheme to the Goodwin Creek Watershed, located in North Mississippi and compare the results with measured erosion rates.

Introduction

The presence of sediment in streams and rivers has its origin in soil erosion. Erosion encompasses a series of complex and interrelated natural processes that have the effect of loosening and moving away soil and rock materials under the action of water, wind, and other geologic factors. In the longterm, the effect of erosion is the denudation of the land surface, ie., the removal of soil and rock particles from exposed surfaces, their transport to lower elevations, and eventual deposition.[2]

That accelerated soil erosion is a serious global problem is widely recognized. What is difficult to assess reliably and precisely, however, are the dimensions - the extent, magnitude, and rate - of soil erosion and its economic and environmental consequences.[1] This paper will describe some of the widely used methods to estimate the overland soil loss based upon the movement of sediment in the upland watersheds due to rainfall - runoff processes.

Universal Soil Loss Equation (USLE)

In the United States, the prediction of upland erosion amounts (ie., sheet and rill erosion) is commonly made by the USLE, developed by the USDA Agricultural Research Service in cooperation with the USDA Soil Conservation Service and certain other state experiment stations.

This method is only able to compute the annual soil loss due to sheet and rill erosion in tons per acre per year. The equation is as follows:

$$A=RKLSCP$$

where,

A = Annual soil loss due to sheet and rill erosion in tons per acre per year.
R = Rainfall factor
K = Soil Erodibility factor
L = Slope-Length factor
S = Slope-Gradient factor
C = Crop-Management factor
P = Erosion-Control-Practice factor

The USLE computes upland erosion from small watersheds on an average annual basis. It includes detachment and transport components, but it does not account for the deposition component. Therefore, the USLE cannot be used to compute sediment yield. For example, in a 1000 square mile drainage basin, only 5 percent of the soil loss computed by the USLE may appear as sediment yield at the basin outlet. The remaining 95 percent is redistributed on uplands or floodplains and does not constitute a net soil loss from the drainage basin.[2]

Rainfall Erosivity Factor

When factors other than rainfall are held constant, soil losses from cultivated fields are shown to be directly proportional to the product of the storm's total kinetic energy (E) and it's maximum 30-minute intensity (I). The product of EI reflects the combined potential of raindrop impact and runoff turbulence to transport dislodged soil particles.

The sum of EI products for a given year is an index of the erosivity of all rainfall for that year. The rainfall factor (R) is the average value of the series of annual sums of EI products.[2] Average values of R for the contiguous United States can be seen in Figure 1.

Soil Erodibility Factor

The soil erodibility factor (K) is a measure of the resistance of a soil surface to erosion. It is defined as the amount of soil loss (in tons per acre per year) per unit of rainfall factor (R) from a unit plot. A unit plot is 72.6 feet long, with a uniform gradient (lengthwise) of 9 percent, in continuous fallow, tilled up and down the slope. Some typical values of K can be seen in Table 1.[2]

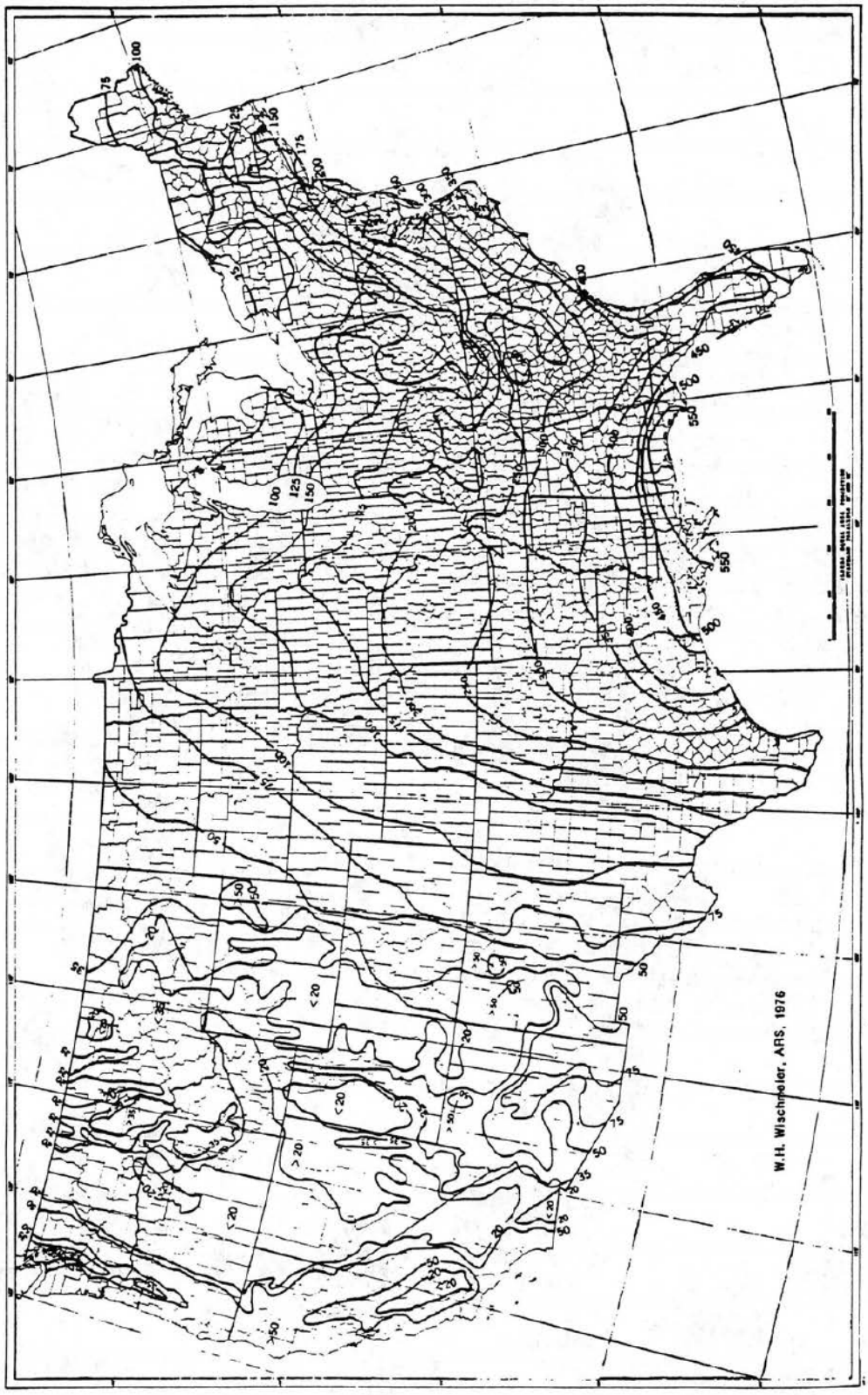

Figure 1 - Rainfall Factor (R) in the Universal Soil Loss Equation.[2]

Soil Type	Source of Data	*K*
Dunkirk silt loam	Geneva, NY	0.69[1]
Keen silt loam	Zanesville, OH	0.48
Shelby loam	Bethany, MO	0.41
Lodi loam	Blacksbrug, VA	0.39
Fayette silt loam	LaCrosse, WI	0.38[1]
Cecil snady clay loam	Watkinsville, GA	0.36
Marshall silt loam	Clarinda, IO	0.33
Ida silt loam	Castana, IO	0.33
Mansic clay loam	Hays, KA	0.32
Hagerstown silty clay loam	State College, PA	0.31[1]
Austin clay	Temple, TX	0.29
Mexico silt loam	McCredie, MO	0.28
Honeoye silt loam	Marcellus, NY	0.28[1]
Cecil sandy loam	Clemson, SC	0.28[1]
Ontario loam	Geneva, NY	0.27[1]
Cecil clay loam	Watkinsville, GA	0.26
Boswell fine sandy loam	Tyler, TX	0.25
Cecil sand loam	Watkinsville, GA	0.23
Zaneis fine sandy loam	Guthrie, OK	0.22
Tifton loamy sand	Tifton, GA	0.10
Freehold loamy sand	Marlboro, NJ	0.08
Bath flaggy silt loam with surface stones greater than 2 in. removed	Arnot, NY	0.05[1]
Albia gravelly loam	Beemerville, NJ	0.03

[1]Evaluated from continuous fallow. All others were evaluated from row-crop data.

Table 1 - Values of Soil Erodibility Factor (K).[2]

Vegetative Canopy		Cover That Contacts the Soil Surface						
			Percent Ground Cover					
Type and Height[2]	% Cover[3]	Type[4]	0	20	40	60	80	100
No appreciable canopy		G	0.45	0.20	0.10	0.042	0.013	0.003
		W	0.45	0.24	0.15	0.091	0.043	0.011
Tall grass, weeds or short brush with average drop fall of 20 in. or less	25	G	0.36	0.17	0.09	0.038	0.013	0.003
		W	0.36	0.20	0.13	0.083	0.041	0.011
	50	G	0.26	0.13	0.07	0.035	0.012	0.003
		W	0.26	0.16	0.11	0.076	0.039	0.011
	75	G	0.17	0.10	0.06	0.032	0.011	0.003
		W	0.17	0.12	0.09	0.068	0.038	0.011
Appreciable brush or bushes, with average drop fall height of 6.5 ft	25	G	0.40	0.18	0.09	0.040	0.013	0.003
		W	0.40	0.22	0.14	0.087	0.042	0.011
	50	G	0.34	0.16	0.08	0.038	0.012	0.003
		W	0.34	0.19	0.13	0.082	0.041	0.011
	75	G	0.28	0.14	0.08	0.036	0.012	0.003
		W	0.28	0.17	0.12	0.078	0.040	0.011
Trees, but no appreciable low brush. Average drop fall height of 13 ft	25	G	0.42	0.19	0.10	0.041	0.013	0.003
		W	0.42	0.23	0.14	0.089	0.042	0.011
	50	G	0.39	0.18	0.09	0.040	0.013	0.003
		W	0.39	0.21	0.14	0.087	0.042	0.011
	75	G	0.36	0.17	0.09	0.039	0.012	0.003
		W	0.36	0.20	0.13	0.084	0.041	0.011

[1]The listed *C* values require that the vegetation and mulch be randomly distributed over the entire area. For grazed forest land, multiply these values by 0.7.

[2]Canopy height is measured as the average fall height of water drops falling from canopy to ground. Canopy effect is inversely proportional to drop fall height and is negligible if fall height exceeds 33 ft.

[3]Portion of total area surface that would be hidden from view by canopy in a vertical projection.

[4]G: cover at surface is grass, grasslike plants, decaying compacted duff, or litter. W: cover at surface is mostly broad-leaf herbaceous plants (weeds) or undecayed residues or both.

Table 2 - Values of Crop-Management Factor (C) for Permanent Pasture, Grazed Forest Land, Range, and Idle Land.[2]

Percentage of Area Covered by Canopy of Trees and Undergrowth	Percentage of Area Covered by Litter[2]	*C* Value[3]
100–75	100–90	0.0001–0.001
70–45	85–75	0.002–0.004
40–20	70–40	0.003–0.009

[1]Where litter cover is less than 40% or canopy cover is less than 20%, use Table 15-5. Also, use Table 15-5 when woodlands are being grazed, harvested, or burned.

[2]Percentage of area covered by litter is dominant. Interpolate on basis of litter, not canopy.

[3]The ranges in listed *C* values are caused by the ranges in the specified forest litter and canopy cover, and by variations in effective canopy height.

Table 3 - Values of Crop-Management Factor (C) for Undisturbed Forest Land.[2]

	For Farm Planning		For Computing Sediment Yield[2]	
Land Slope (percent)	Contour Factor[3]	Strip-crop Factor	Graded Channels, Sod Outlets	Steep Backslope, Underground Outlets
1–2	0.60	0.30	0.12	0.05
3–8	0.50	0.25	0.10	0.05
9–12	0.60	0.30	0.12	0.05
13–16	0.70	0.35	0.14	0.05
17–20	0.80	0.40	0.16	0.06
21–25	0.90	0.45	0.18	0.06

[1]Slope length is the horizontal terrace interval. The listed values are for contour farming. No additional contour factor is used in the computation.

[2]These values include entrapment efficiency and are used for control of offsite sediment within limits and for estimating the field's contribution to watershed sediment yield.

[3]Use these values for control of interterrace erosion within specified soil-loss tolerances.

Table 4 - Values of Erosion-Control-Practice Factor (P) for Contoured-Farmed Terraced Fields.[2]

Length-Slope Factor

The rate of soil erosion by flowing water is a function of slope length (L) and gradient (S). For practical purposes, these two topographic characteristics are combined into a single topographic factor (LS). The topographic factor is defined as the ratio of soil loss from a slope of given length and gradient to the soil loss from a unit plot (of 72.6 feet in length and 9 percent gradient).[2] The following equation can be used to compute the LS factor.[3]

$$LS = X_r^{0.5}(0.0076 + 0.53S_o + 7.6S_o^2)$$

where,

LS = Length-Slope Factor
X_r = Runoff Length (Feet)
S_o = Gradient (Feet/Feet)

Crop Management Factor

The Crop Management Factor (C) is defined as the ratio of soil loss from a certain combination of vegetative cover and management practice to the soil loss resulting from tilled, continuous fallow. Values of C range from as little as 0.0001 for undisturbed forest land to a maximum of 1.0 for disturbed areas with no vegetation. Values of C for cropland are estimated on a local basis. Table 2 shows values of C for permanent pasture, grazed forest land, range, and idle land. Table 3 shows values of C for undisturbed forest land.[2]

Erosion Control Practice Factor

The Erosion Control Practice Factor (P) is defined as the ratio of soil loss under a certain erosion control practice to the soil loss resulting from straight row farming. Practices for which P have been established are contouring and contour strip-cropping. In contour strip-cropping, strips of sod or meadow are alternated with strips of row crops or small grains. Values of P used for contour strip-cropping are also used for contour-irrigated furrows. Table 4 shows values of P for contour-farmed terrace fields.[2]

Revised Universal Soil Loss Equation (RUSLE)

The USLE has been the workhorse of the erosion prediction and conservation planning technology in the U.S. and even worldwide. In 1985, at a meeting of the USDA and other erosion researchers, it was decided that the USLE should be revised to incorporate additional research and technology developed after the 1978 USLE handbook. The result of this effort was the RUSLE.[1]

RUSLE maintains the basic structure of the USLE, namely,

$$A=RKLSCP$$

This empirically based equation, derived from a large mass of field data, computes sheet and rill erosion using values representing the four major factors affecting erosion. These factors are climate erosivity represented by R, soil erodibility represented by K, topography represented by LS, and land use and management represented by CP.[1]

Whereas the basic USLE structure has been retained, the algorithms used to calculate the individual factors have been changed significantly in RUSLE. New climatic erosivity values have been calculated which reflect the variability of R in the mountainous conditions of the western U.S. The soil erodibility factor, K, is varied seasonally being highest in spring and lowest in fall synonymous with soil freezing. The topographic factors, L and S, are evaluated using four separate slope length relationships. The soil loss ratios are calculated with time dependent functions that address subfactors reflecting prior land use, crop canopy, surface or ground cover, and surface roughness. Finally, the conservation practice value represents broad, general effects of such practices as contouring, strip cropping, subsurface drainage, and terracing. P-factors have also been developed to reflect conservation practices on rangeland and require the user to estimate surface roughness and runoff reductions.[1]

R-Factor

The rainfall-runoff erosivity term in RUSLE is calculated as the product of storm kinetic energy times the maximum 30-minute storm depth and summed for all storms in a year. The R-factor represents the input drives the sheet and rill erosion processes. Thus differences in R values represent differences in erosivity of the climate. Of all the RUSLE factors, R is the one most exactly computed from input data.[1]

In the western U.S., new R values have been calculated using over 1000 point values, a significant addition to the information available in "Agriculture Handbook 537". Whereas the old R isoerodent maps for the west had maximum point values of about 50 units (hundreds of foot-tonforce-inch/acre-hour-year), new values are as large as 350 units along the Pacific coastal areas. Some changes are also involved in the eastern U.S. (east of the 105th meridian). Another change in the R-factor is to reduce R values where flat slopes occur in regions of long intense rainstorms. Ponded water on the soil reduces the erosivity of the rain. Finally, an R equivalent approach is being used in the frozen soil areas of the Pacific Northwest to reflect the combined effect of rain or snowmelt on frozen or partly-thawed soil.[1]

K-Factor

The K-factor is a measure of the inherent erodibility of a given soil under standard condition of the unit USLE plot maintained in continuous fallow. Values for K typically range from 0.10 to 0.45 (U.S. customary units), with high-sand and high-clay content soils having the lower values and high-silt soils having the higher values. Users have little difficulty choosing a K-factor value because the Soil Conservation Service (SCS) has identified K values for all major soil mapping units in the U.S. However, the site-specific K value, and it's seasonal variation, can be quite different from the K value given in the soil survey information.[1]1

RUSLE varies K seasonally, a major change over the USLE procedure. Experimental data show that K is not constant but varies with season, being highest in early spring and lowest in mid-fall or when the soil is frozen. The seasonal variability is addressed by weighing the instantaneous estimate of K in proportion to EI (the percent of annual R) for twice monthly intervals. Instantaneous estimates of K are made from equations relating K to the frost-free period and the annual R-factor.[1]

An additional change incorporated in RUSLE is to account for rock fragments on and in the soil, a common occurrence on western rangelands. Rock fragments on the soil surface are treated like mulch in the C-factor, while K is adjusted for rock in the soil profile to account for effects on runoff.[1]

LS-Factor

More questions and concerns are expressed over the L-factor than any of the other USLE factors. One reason is that the choice of a slope length involves judgement; different users choose different slope lengths for similar situations. RUSLE includes improved guides for choosing slope length values to give greater consistency among users. RUSLE uses four separate slope length relationships. Three are functions of slope steepness as in the USLE, and of the susceptibility of the soil to rill erosion relative to interrill erosion. A slope length relationship has also been developed specifically for the frozen soil area of the Pacific Northwest of the U.S.

C-Factor

The C-factor is perhaps the most important USLE/RUSLE factor because it represents conditions that can most easily be managed to reduce erosion. Values of C can vary from near zero for a very well protected soil to 1.5 for a finely tilled, ridged surface that produces much runoff and leaves the soil highly susceptible to rill erosion.[1]

Soil loss ratios vary during the year as soil and cover conditions change. To compute C, soil loss ratios (SLR) are weighted according to the distribution of erosivity during a year (ie., from the information in the city code and climate data). In RUSLE, a subfactor method is used to compute SLRs as a function of four subfactors given as:[1]

$$C = PLU * CC * SC * SR$$

where,

C = C-factor
PLU = prior land use
CC = crop canopy
SC = surface or ground cover
SR = surface roughness

In the Pacific Northwest area where fallow is used to replenish soil moisture, the additional term is included reflecting the moisture status of the profile.

In "Agriculture Handbook 537", SLRs were given in several tables for differing crops and crop growth periods. In many instances, the SLRs were developed for row spacing, crop varieties, and practices no longer used and in other instances, the SLRs were just not available. In the RUSLE approach, with a farming operation and crop file for which fundamental data are available, SLRs can be calculated and weighted at 15-day intervals to obtain a crop or annual cover-management factor.

P-Factor

Of the USLE/RUSLE factors, values for the P-factor are the least reliable. The P-factor mainly represents how surface conditions affect flow paths and flow hydraulics. For example, the contouring, runoff flows around the slope in channels formed by tillage. The grade and flow velocities could be much lower than in up-and-down hill flow paths. There are many interacting variables that determine the effect of contouring. Size of storm, antecedent soil water, and tillage type to name a few of these variables, interact in such a way that a contouring factor may vary widely from storm to storm and field to field. Thus, P-factor values represent broad, general effects of such practices as contouring.[1]

RUSLE P-factors are treated as the product of subfactors computed based on practices applied to the landscape. In RUSLE, extensive data (both field and model) have been analyzed to reevaluate the effect of contouring. The results have been interpreted to give factor values for contouring as a function of ridge height, furrow grade, and climate erosivity. New P-factor values for the effect of terracing account for grade along the terrace while a broader array of strip-cropping conditions are considered in RUSLE than in USLE.[1]

Finally, P-factors in RUSLE have been developed to reflect conservation practices on rangelands. The practices require estimates of surface roughness and runoff reduction.[1]

Modified Universal Soil Loss Equation (MUSLE)

Williams and Berndt (1972) recognized that application of the USLE is limited to soil loss, and developed another procedure for computing sediment yields from watersheds. This method determines sediment yield based on single storm events from watersheds. They introduced a runoff factor instead of rainfall energy into the USLE to establish soil loss. This makes the MUSLE more applicable to the arid regions of the West, since the effect of short-duration, high-intensity events can be more adequately represented. The MUSLE is

$$Y_s = a(Q_v q_p)^{\beta} KLSCP$$

where Y_s is the sediment yield in tons for the storm event, Q_v is runoff volume in acre-feet, q_p is the peak flow rate in cubic feet per second, a and β are coefficients and the other terms are as defined above.[4]

The coefficients were calibrated as 95 for a and 0.56 for β in watersheds in Texas and Nebraska. These coefficients vary and must be calibrated and verified in other locations.[4]

If the sediment yield from the land surface on an annual basis rather than a single storm event is desired, the MUSLE can also be used. This application is accomplished by determining the soil loss for events of varying return periods. Recommended return periods are 2, 10, 25, 50, and 100 years. The sediment yields are then weighted according to their incremental probability, resulting in a weighted storm average.[4]

To compute the annual yield, the weighted storm yield is multiplied by the ratio of annual water yield to an incremental probability-weighted water yield. For the return periods recommended, the computation is:[4]

$$A_s = \frac{Q_A(0.01Y_{s100} + 0.01Y_{s50} + 0.02Y_{s25} + 0.06Y_{s10} + 0.4Y_{s2})}{0.01Q_{v100} + 0.01Q_{v50} + 0.02Q_{v25} + 0.06Q_{v10} + 0.4Q_{v2}}$$

where, A_s is the annual sediment yield, Q_A is the average annual water yield, and the numerical subscripts in the single storm event Y_s and water yield Q_v refer to the return period of the storm.

Case Study - Evaluation of MUSLE on the Goodwin Creek Watershed

Description of Study Area

The Goodwin Creek Watershed, Figure 2, is approximately 8.2 square miles (5242 acres) which is extensively gaged by the Agricultural Research Service located in Oxford, Mississippi. Goodwin Creek is a sub-watershed of the Long Creek Watershed and is located approximately 60 miles due south of Memphis, Tennessee.

The predominant soil texture for this watershed is silt loam with a small percentage of very fine sandy loam present. The landuse is primarily pasture with some forest and to a small extent row crop.

Methodology

In performing this case study, three storm events were used to calibrate and verify the MUSLE. Storm event 1 started at 9:19 pm on October 17, 1981 with a rainfall duration of 3.52 hours. The peak discharge measured at the outlet was 1405.1 cfs and the volume of runoff was 320.56 acre-feet. Storm event 2 started at 12:00 am on September 30, 1985 with a rainfall duration of 6.0 hours. The peak discharge at the outlet was 158.0 cfs and the volume of runoff was 63.31 acre-feet. Storm event 3 started at 8:31 pm on December 27, 1988 with a rainfall duration of 8.6 hours. The peak discharge was 1218.6 cfs and the runoff volume was 524.0 acre-feet.

From previous studies, the average slope for the Goodwin Creek watershed was computed to be 0.014, the USLE parameters were computed to be: R=330, K=0.478 Tons/Acre, C=0.098, P=1.0, while the runoff length was computed to be 24272 feet. From this data, the LS-factor was computed to be 2.572.

When using the MUSLE, the coefficients (a and β) must be calibrated for the watershed or regional coefficients must be used. For this analysis, storm event 1 was used to calibrate the coefficients and storm events 2 and 3 were used to verify the MUSLE.

In performing the calibration, since a limited amount of data was used, the coefficient (a) was set to be 95 and the coefficient (β) was computed using known values of peak flow, runoff volume, USLE parameters, and measured sediment load. At this point, it should also be noted that the measured sediment load had to be adjusted so that the proper comparison could be made with the MUSLE. The measured value was the total sediment load (wash load and bed load) passing through the outlet. It also reflected sediment storage taking place within the watershed. The MUSLE only computes the wash load and does not take into account any sediment storage. So the measured value was adjusted as follows:

$$Y_s = \frac{Q_e}{SDR} E$$

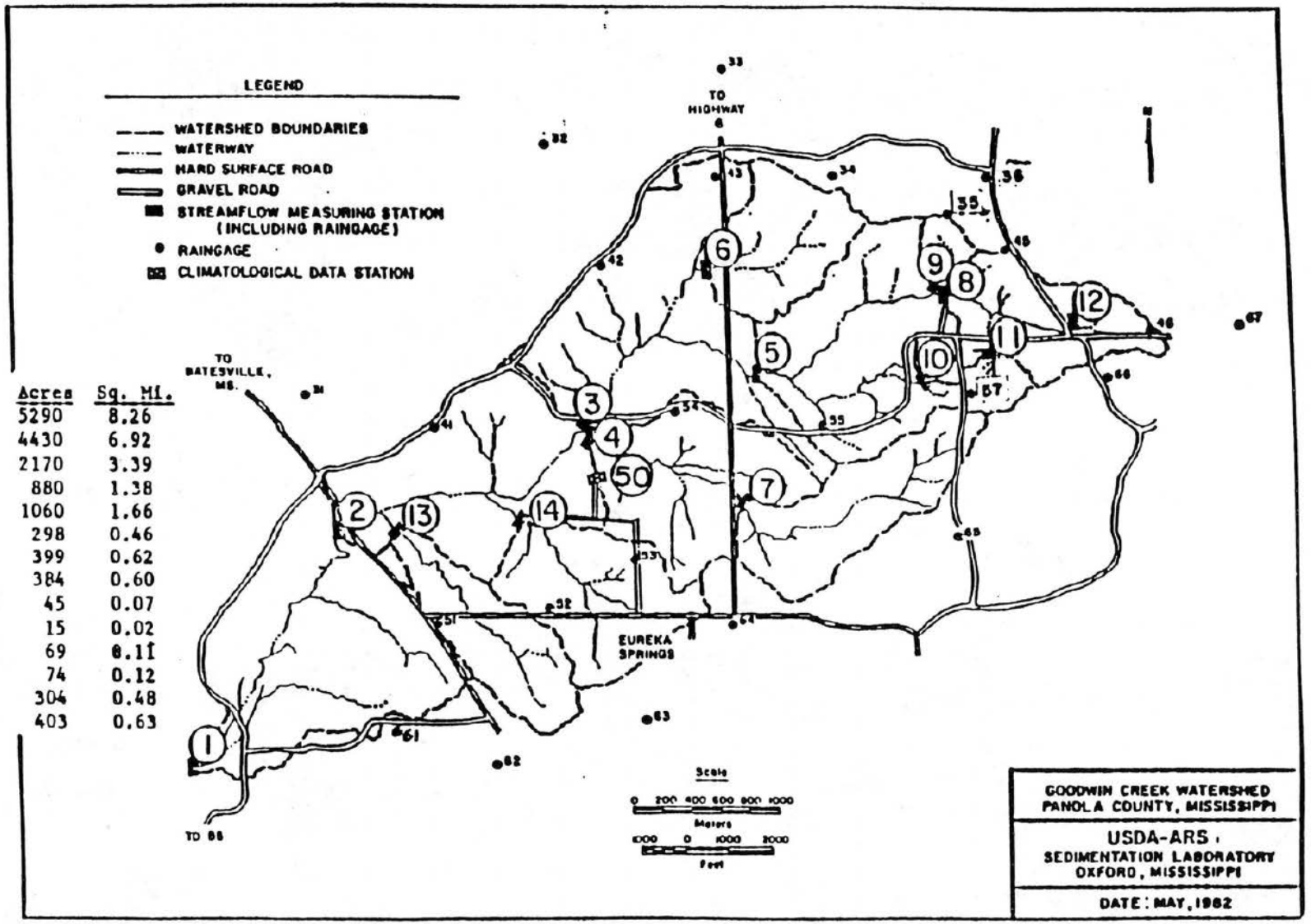

Sta.	Acres	Sq. Mi.
1	5290	8.26
2	4430	6.92
3	2170	3.39
4	880	1.38
5	1060	1.66
6	298	0.46
7	399	0.62
8	384	0.60
9	45	0.07
10	15	0.02
11	69	0.11
12	74	0.12
13	304	0.48
14	403	0.63

Figure 2 - Goodwin Creek Watershed

$$Y_{s_w}=0.4Y_s$$

where,

E = Total Measured Sediment Load (Tons)
Q_e = Grid Size Factor = 0.439
SDR = Sediment Delivery Ratio = 0.163
Y_s = Total Amount of Sediment Eroded (Tons)
Y_{sw} = Total Amount of Wash Load (Tons)

The ARS has estimated that the wash load is approximately 40% of the total load.

Study Results

From performing the calibration analysis, β was computed to be 0.38. The following is a listing of the computed versus the measured sediment loads (Y_{sw}).

Storm Event	Measured Sediment Load (Tons)	Computed Sediment Load (Tons)	Per Cent Difference
1	1515.2	-----	-----
2	82.4	379.2	360.2
3	1282.2	1839.8	43.5

Conclusions

The per cent difference was positive for both storm events used in the verification analysis. If more data had been used, then the MUSLE coefficients could have been better defined and should have provided better results. However, given the gross estimate of the coefficients, the MUSLE still was within an order of magnitude of the measured sediment load. So this method is relatively simple to use and does give relatively good estimates of sediment load on an event basis.

References

1. Lal, R., 1994, Second Edition Soil Erosion Research Methods, Soil and Water Conservation Society, St. Lucie Press, Delray Beach, FL.

2. Ponce, Victor Miguel, 1989, Engineering Hydrology - Principles and Practices, Prentice Hall Inc, Englewoods Cliffs, NJ.

3. Julien, Pierre Y., 1995, Erosion and Sedimentation, Cambridge University Press, New York, NY.

4. Simons, Daryl B., and Senturk, Fuat, 1992, Sediment Transport Technology, Water Resources Publications, Bookcrafters Inc., Chelsea, MI.

5. Overton, Donald E., 1992, Soil Erosion and Sediment Yield - Modeling, Simulation, and Prediction, Stormwater Publications Inc., Knoxville, TN.

6. Noss, Darcy K., 1995, Estimating Upland Erosion Using the Universal Soil Loss Equation - Application to Goodwin Creek, Panola County, MS., Essays on River Mechanics (1995), Colorado State University.

7. Maidment, David R., 1993, Handbook of Hydrology, McGraw-Hill Inc., New York, NY.

Flow-Duration Curves for the Practicing Engineer

Mitchell R. Delcau

The flow-duration curve has long been a tool for the hydraulic/hydrologic engineer to study the flow characteristics of streams. Uses of the flow-duration curve include sedimentation analysis, waterpower studies, environmental stream studies, and basin comparison analysis. In the typical design of a flow-duration curve, the daily, weekly, or monthly average flows are used to determine the percent of time the during which a range of flows are equaled or exceeded for these periods of return for a given drainage basin. Much of this design method is traditionally passed from engineer to engineer. Of course all variations still use the basic process developed by Searcy of U.S.G.S in his 1959 paper "Flow-Duration Curves". However, with the many technological advancements since this paper's origin, the design method for developing flow-duration curves has not been well written in a form for the practicing engineer to use. This paper will develop a design for flow-duration curves for the practicing engineer utilizing new computer technology and practice. In addition, it will address the question of whether developing daily, weekly, or monthly curves are accurate enough for suitable modern hydrologic/hydraulic designs or whether 1-hour or 6-hour duration curves should be used. The method of analysis will be the classical total-period method. In which, all discharges are classified into separated divisions based on their magnitudes. The totals are cumulated and the percentage of the totaled time each division is equaled or exceeded is computed. This is the method adopted by the U.S.G.S. and is widely accepted in practice.

Data Collection:

To design duration curves, a gauged site is needed for the drainage basin. In most cases, these are usually operated by the U.S.G.S. or the U.S. Army Corps of Engineers. To obtain the flow data for a given site, it is helpful to know several details of the location where the gauge lies. These are: 1) Name of the bridge, town, or lock and dam, etc. 2) Latitude and Longitude of the gauge site 3) Gauge number. From any of these parameters or a combination of them, the engineer from a federal agency (U.S.G.S. or Corps) can provide the data needed in digital ASCII format. A typical heading in a database for a gauge would appear as the following:

UNITED STATES DEPARTMENT OF THE INTERIOR -
GEOLOGICAL SURVEY - MONTANA
STATION NUMBER 06088500
MUDDY CREEK AT VAUGHN, MT. STREAM SOURCE AGENCY USGS
LATITUDE 473342 LONGITUDE 1113233
DRAINAGE AREA 391.00
DATUM 3337.6
STATE 30 COUNTY 013

For most cases, this data can be provided for 1-hour, 6-hour, 1-day, 1-month, and 1-year

intervals. It may take some time to receive this information from these agencies depending on the workload for their engineers. A fee may also be assessed as well. Therefore, if the design allows for daily average flows or greater intervals, the data can be taken from the Internet. The U.S.G.S. has an Internet address at: http://h2o.usgs.gov/swr/. By knowing any of the information discussed subsequently, the engineer can establish a direct connection to the gauge information. The year as well as the desired month may be specified and an ASCII file created in which to download the data. This procedure will not be discussed, but consult a local Internet expert or text and it is not hard to learn.

Once the flow data is acquired, it will be imported into a spreadsheet software package. The two most common packages utilized are Borland's Quattro Pro for Windows or Microsoft Excel for Windows. However, any other software package may used as long as there are analysis tools to analyze the data within the package. The ensuing design procedure will assume the engineer has some computer knowledge of windows computer packages.

Hydrologic Analysis:

To import the data in Excel, simply go to the **file** menu and open the file as a text file and the program will allow for immediate parsing of the data (dividing the ASCII text into columns). For Quattro Pro, the data must be imported under the **tools** menu. Quattro parses the data automatically, if when the file is opened it is specified as a tab delimitated text file. With the flow data imported to the spreadsheet, it will need to be ordered in a certain manner for use of the spreadsheet's analysis tools. First, it has been found easier to analyze, if the data is distributed by columns of either 1-day, 1-year, etc. as seen below:

1980	1981	1982	1983	1984	1985	1986
77	76	75	74	74	75	76
78	78	77	77	77	77	76
77	76	75	75	78	80	83
84	86	87	87	87	90	91
84	83	79	78	78	78	78
82	82	83	84	83	83	83
85	87	87	87	89	89	89

There can be no blank cells in the columns vertically or horizontally. This means, there can be no blank columns separating each day or year, etc. If the data is not compacted the analysis tools program **will not** complete its computations.

The histogram analysis will be performed on the data. This is the analysis the U.S.G.S. specifies as the total-period method. For this method all flows will be distributed into 20-30 class intervals. Generally in practice, 30 intervals are selected into which the flows are distributed. However, this actually means 33 intervals because the U.S.G.S. defines 0-0, 0-lowest flow, and last flow to highest flow intervals additionally to the defined 30. The intervals for distribution are determined using the following equation:

$$interval = \frac{LOG(highest\ flow) - LOG(lowest\ flow)}{33}$$

This will compute a log interval number for distribution. To calculate the next interval, add this number to the lowest flow. Then, add the interval number to that number, etc. This can be done using a formula which is copied downward from cell to cell in the spreadsheet. Remember, there is a 0-0 interval and a 0 - lowest flow interval. Therefore, start adding this log interval in a cell following a computation of the log of the lowest flow. In a column adjacent to the class intervals just computed, convert the log discharges to actual discharges by raising each discharge to 10^x. Where x is the log discharge. Enter these columns below the cells on the spreadsheet containing the flow data to be analyzed. For example if the highest flow in the data set is 1610 cfs and the lowest flow is 9.7 cfs, the columns should look approximately like the ones below:

Interval	A	B
0.067	0	0
	0.99	9.7
	1.05	11.33
	1.12	13.22
	1.19	15.44
	1.26	18.02
	1.32	21.04
	1.39	24.57
	1.46	28.69
	1.52	33.49
	1.59	39.11
	1.66	45.66
	1.73	53.31
	1.79	62.24
	1.86	72.67
	1.93	84.84
	2.00	99.06
	2.06	115.65
	2.13	135.03
	2.20	157.66
	2.26	184.07
	2.33	214.91
	2.40	250.92
	2.47	292.96
	2.53	342.04
	2.60	399.35
	2.67	466.26
	2.74	544.38
	2.80	635.59
	2.87	742.09
	2.94	866.42
	3.01	1011.59
	3.07	1181.07
	3.14	1378.96
	3.21	1610.00

- The column labeled interval is the interval obtained using the above equation.

- Column A is the interval added from the lowest flow to the highest flow.

- Column B is the actual interval distribution of discharges which are the values in column A computed as Q= 10^x.

- *Note: The first row in columns A & B is the 0-0 interval and the second row is the 0 - lowest flow interval. Therefore, the cell which contains 1.05 is the first cell in which 0.067 is added.
If checking these values, remember the spreadsheet is carrying more decimal places.

After establishing the class intervals, the next step is to perform a histogram analysis on the data. To execute this procedure, the analysis tools for the spreadsheet must be initiated. In Excel, go to the **tools** menu and click on data analysis. This will bring up a list of analysis tools. Pick the histogram tool. In Quattro Pro, the tools are also initiated from the **tools** menu. Click on analysis tools. Simultaneously, several other icons will appear under the icons at the top of the screen. One will have a picture of a histogram on it. To start the histogram analysis click this icon. Both in Excel and Quattro Pro, a screen will appear and prompt for: input range, bin range, and output range. The input range will be from the start of the first cell a discharge is entered to the last cell containing a discharge. The bin range (class intervals) will be from the 0-0 bin in column B to the highest flow in column B. The output range can be anywhere on the sheet, but it is generally placed several columns to the right of the class interval columns. After entering the ranges, click the **OK** button and the spreadsheet will perform the analysis for the discharges entered on the sheet. The output should appear in the range specified on the histogram analysis and will look similar to the spreadsheet on the left.

Flows	*Frequency*	*% Frequency*
0	0	0
9.7	54	0.01
11.33	163	0.03
13.22	130	0.02
15.44	260	0.04
18.02	477	0.08
21.04	280	0.04
24.57	340	0.05
28.69	442	0.07
33.49	200	0.03
39.11	166	0.03
45.66	223	0.04
53.31	240	0.04
62.24	152	0.02
72.67	402	0.06
84.84	345	0.06
99.06	189	0.03
115.65	173	0.03
135.03	84	0.01
157.66	92	0.01
184.07	284	0.05
214.91	471	0.08
250.92	351	0.06
292.96	233	0.04
342.04	110	0.02
399.35	62	0.01
466.26	64	0.01
544.38	76	0.01
635.59	41	0.01
742.09	42	0.01
866.42	24	0.00
1011.59	30	0.00
1181.07	20	0.00
1378.96	16	0.00
1610.00	9	0.00
total Q's	6245	1

- The flows column contains the actual discharge intervals.

- The frequency column is the number of times the histogram analysis found this flow on the given input range of the spreadsheet.

- The % frequency column is the number of times the flow occurs divided by the total of discharges. IE: 54/6245 is equal to 0.01.

- This data can be plotted by using the graphing tools in either Excel or Quattro Pro. The flow-duration curve is the plot of the flows column versus the % frequency column. It is acceptable in practice to plot either the discharge on the x-axis or the y-axis. However, most curves are plotted with the frequency of occurrence presented as the % of the time the discharge is exceeded. This is done by subtracting the values in the % frequency column from 1. For example, in the range of 9.7 to 11.33 cfs, these discharges occur 54 times in the data, or have % frequency of 0.01 occurrence. But, the % of the time these discharge will be exceeded is 0.99 or 99%.

- It is good practice to check the % frequency column, making sure its total is 1. This will insure the analysis is correct and all flows entered into the data set are included.

Comparison of Flow-Durations:

Depending on the data available, a major concern with the development of a flow-duration curve is the time increment it upon which it is developed. In the past, most curves have been designed for daily or yearly averaged flows. However, a major concern with these increments is whether higher or lower discharges are accurately accounted for in the analysis. A cursory research is performed on Muddy Creek in Montana to aid in this important issue. For the water year 1994-1995, 1-hr, 6-hr, and 1-day average duration curves were designed. From the analysis, the following results are obtained. One detail is readily seen. This is the high and low discharges associated with each time increment. Depending on the type of analysis the duration curve will be needed, this may or may not prove to be significant. For instance, the curve could be used for a flow-duration/sediment rating curve. If the 1-hr curve is used a peak discharge of 1610 cfs is included. However, the 6-hr and 1-day curves would provide values of 1392 and 818 cfs respectively. The impact of how much sediment this stream could transport would be slightly different, although within an order of magnitude. However, if the curve is used for environmental restoration purposes, it may be essential to better define closely the upper and lower limits of the curve.

1-hr		6-hr		1-day	
0.00	0.0	0	0.0	0	0.0
9.70	0.9	6.12	0.1	11.08	0.3
11.33	2.6	7.21	0.3	12.62	1.2
13.22	2.1	8.50	0.0	14.38	0.9
15.44	4.2	10.02	1.1	16.38	3.2
18.02	7.6	11.81	1.6	18.66	2.9
21.04	4.5	13.93	2.2	21.26	1.7
24.57	5.4	16.42	6.8	24.22	4.3
28.69	7.1	19.35	6.9	27.60	4.3
33.49	3.2	22.81	4.4	31.44	2.3
39.11	2.7	26.89	10.3	35.81	2.0
45.66	3.6	31.69	4.7	40.80	2.3
53.31	3.8	37.35	2.6	46.48	4.3
62.24	2.4	44.03	4.9	52.95	3.5
72.67	6.4	51.90	3.9	60.33	2.6
84.84	5.5	61.18	2.4	68.73	5.8
99.06	3.0	72.11	7.6	78.30	4.3
115.65	2.8	85.00	7.0	89.20	2.6
135.03	1.3	100.20	2.6	101.62	2.3
157.66	1.5	118.11	1.7	115.76	3.5
184.07	4.5	139.22	0.6	131.88	1.7
214.91	7.5	164.10	1.9	150.25	2.6
250.92	5.6	193.43	4.4	171.17	3.5
292.96	3.7	228.00	6.7	195.00	8.1
342.04	1.8	268.76	5.2	222.15	7.8
399.35	1.0	316.79	3.1	253.08	7.2
466.26	1.0	373.42	1.1	288.32	4.9
544.38	1.2	440.16	1.2	328.46	4.0
635.59	0.7	518.84	0.8	374.19	1.2
742.09	0.7	611.57	1.7	426.29	1.7
866.42	0.4	720.88	0.4	485.65	1.4
1011.59	0.5	849.73	0.6	553.27	0.6
1181.07	0.3	1001.62	0.6	630.30	1.2
1378.96	0.3	1180.64	0.2	718.06	0.3
1610.00	0.1	1391.67	0.4	818.04	0.3

Conclusions:

The presented method for designing flow-duration curves is used by many practicing engineers. It is based on the methods set forth by the U.S.G.S. written by Searcy. It should be noted this procedure is biased since it involves using logarithms to develop interval distribution. Other modern techniques are vastly being evaluated using non-parametric approaches. However, the presented process is still acceptable in hydrologic and hydraulic design. Based on evaluating smaller time increments than 1-day for the design of the flow-duration curve, it has been observed that major differences are not seen in the curves. But, it should be noted that upper and lower ends of the curves can be better defined with smaller time scales. However, if the data for 1-hr and 6-hr is not available, daily data can provide a reasonable design for the duration curve. Further research should be conducted in this area to provide more substantial justification for these results.

References

Crawford, C.G., 1991. Estimation of suspended-sediment rating curves and mean suspended-sediment loads. Journal of Hydrology, 129:331-348

Julien, P.Y., 1995. Erosion and Sedimentation, Cambridge University Press

LeBoutiller, D.W., Waylen, P.R. 1993. A Stochastic Model of Flow Duration Curves, Water Resources Research, 29(10):3535-3541

Lopes, V.L., Ffolliott, P.F. 1993. Sediment Rating Curves for a Clearcut Ponderosa Pine Watershed in Northern Arizona, Water Resources Bulletin, 29(3):369-382

Searcy, J.K., 1959. Flow-Duration Curves, Geological Survey Water-Supply Paper, 1542-A

Simons, D.B., Senturk, F., 1992. Sediment Transport Technology Water and Sediment Dynamics, Water Resources Publications

Singh, K.P., Durgunoglu, A. 1992. Predicting Sediment Loads. Civil Engineering, 64-65

Vogel, R.M., Fennessey, N.M., 1994. Flow Duration Curves I: A New Interpretation and Confidence Intervals. Journal of Water Resources Planning and Management, ASCE 120(4):485-504

Vogel, R.M., Fennessey, N.M., 1995. Flow Duration Curves II: A Review of Applications in Water Resources Planning. Water Resources Bulletin 33(6):1029-1039

COMPARISONS OF A VELOCITY PROFILE MODEL WITH EXPERIMENTS FOR SEDIMENT-LADEN FLOWS

Junke Guo

Department of Civil Engineering

Colorado State University

Fort Collins, CO 80523

April 14, 1996

ABSTRACT

In this small project, a turbulent velocity profile model suggested by this author is compared with Coleman's flume experimental data. The results show that the model fits the experimental data very well in the entire flow depth except the laminar sublayer which is very near the bottom. From the plots, it can be seen that the Karman constant κ decreases with the presence of sediment particles; while the effects of sediment on the mixing length strength m is not very obvious.

I. INTRODUCTION

The velocity profile of sediment-laden flows in open channels is one of the most important subjects in alluvial hydraulics and sediment transport. For the last 50 years, there have been many experimental investigations. Most experiments showed that the Prandtl log law can not been directly used for sediment-laden flows. For example, Vanoni (1946), Einstein and Chien (1955) argued that if the log law is applied to sediment-laden flows, the Karman constant κ must be reduced by the presence of sediment particles. Others, like Coleman (1981, 1986), believed that the above conclusion was obtained by misunderstanding the log law. They argued that the log law is only valid in the inner region, i.e., close bed region; when the log law is extended to the outer region, a wake function term suggested by Coles (1956) must be added. If the wake function term is considered, the Karman constant κ may be kept the same as that for clear water, the presence of sediment particles only modifies the Coles wake strength Π instead of the Karman constant κ. Later, Lyn (1988) applied the similarity principle to sediment-laden flows and concluded that the sediment particles may affect both Karman constant κ and Coles wake strength Π. Guo (1988) believed that the key to resolving the above conflict is to understand what the physical meanings of κ and Π are. He reexamined the Prandtl's mixing length hypothesis using the modern turbulent experiments and suggested a general velocity profile equation, which contains two parameters κ and m. He further pointed out that the Karman constant κ expresses the intensity of vertical velocity fluctuation; while parameter m represents the strength of mixing length, which is equivalent to the Coles wake strength Π. So far, It is still difficult to judge which one has an advantage over the others. In this project, a detailed discussion of these models' majors and minors is left out. Only the comparisons of Guo's equation with Coleman's experiments will be emphasized.

II. VELOCITY PROFILE MODEL

Guo (1988), by reexamining the Prandtl's mixing length hypothesis with modern turbulent experiments, derived the following velocity profile equation:

$$\frac{u_{\max}-u}{u_*}=\frac{m}{\kappa}\left[\sum_{i=0}^{\infty}\frac{(1-\xi)^{2+mi}}{2+mi}-(1-\xi_{\max})\sum_{i=0}^{\infty}\frac{(1-\xi)^{1+mi}}{1+mi}\right]_{\xi_{\max}}^{\xi} \tag{1}$$

in which κ and m are parameters; ξ is the normalized distance from the bottom $\left(=\frac{z}{h}\right)$; and $\xi_{\max}$ is the position of the maximum velocity. He further noted that the Karman constant κ expresses the vertical fluctuation intensity; and m represents the strength of mixing length. The above equation can be approximated as

$$\frac{u_{\max}-u}{u_*}=\frac{m}{2\kappa}\left\{(\xi_{\max}-\xi)^2-\frac{2(1-\xi)(\xi_{\max}-\xi)}{m}\ln\left[1-(1-\xi)^m\right]\right\} \tag{2}$$

If the maximum velocity occurs at the water surface, $\xi_{\max}=1$, the above equation can be further simplified as

$$\frac{u_{\max}-u}{u_*}=\frac{m}{2\kappa}(1-\xi)^2\left\{1-\frac{2}{m}\ln\left[1-(1-\xi)^m\right]\right\} \tag{3}$$

Special cases ($\xi_{\max}=1$):

- If $\xi \ll 1$, (2) or (3) can be simplified as the log law, i.e.

$$\frac{u_{\max}-u}{u_*}=-\frac{1}{\kappa}\ln\xi \tag{4}$$

- If $1-\xi \ll 1$, (2) or (3) can be simplified as the parabolic law, i.e.

$$\frac{u_{\max}-u}{u_*}=\frac{m}{2\kappa}(1-\xi)^2 \tag{5}$$

  Note that this equation is also valid for the case of $\xi_{\max}<1$.

- If we expand (2) or (3) at $\xi=0$, an equivalent log-wake law can be obtained as follows:

$$\frac{u_{\max}-u}{u_*}=-\frac{1}{\kappa}\ln\xi+w(\xi,m) \tag{6}$$

  in which the wake function $w(\xi,m)$ is a Taylor series, and m is equivalent to the Coles wake strength Π.

III. COMPARISONS WITH COLEMAN'S EXPERIMENTS

Coleman (1981, 1986) reported 40 sets of data of flume experiments. The experiments were performed in a recirculating flume with a rectangular Plexiglas channel 356mm wide and 15 m long, with slope adjustment capability for maintaining uniform flow. During the experiments, the discharges were kept to be 0.064 m^3/s; flow depth between 167 mm and 174 mm; energy sloe 0.002; temperature between 21°C and 24°C; shear velocity 0.041 m/s. Only sediment concentrations varied in each experiment such that we could isolate the effects of concentration on velocity profiles.

Only the first 20 runs of Coleman's experiments are used in this project. The data analysis procedure is as follows: (1) Based on equation (5), assume the velocity profile near water surface satisfies the parabolic law, then we can find the maximum velocity and its position by using the curve-fitting method; (2) Once the maximum velocity and its position have been known, only two parameters, m and κ in equation (2) are required. We use the following criterion to optimize the values of m and κ:

$$\text{Minimize:} \quad Err = \sum_{i=1}^{n} \left(1 - \frac{u(y_i, m, \kappa)}{u_i}\right)^2 \tag{7}$$

in which n is the sample number; u is the theoretical velocity at point y_i; and u_i is the measured velocity at y_i; and (3) Plot the theoretical velocity profiles and calculate the associated coefficient r. A MatLab code (see Appendix) has been written to carry out the above steps, the results are plotted in Figs. 1-20 (RUNS 1-20).

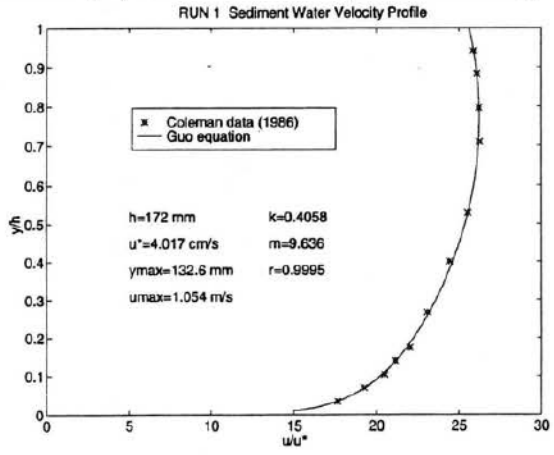

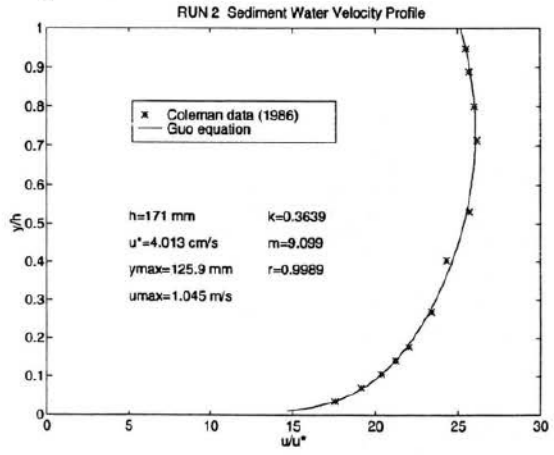

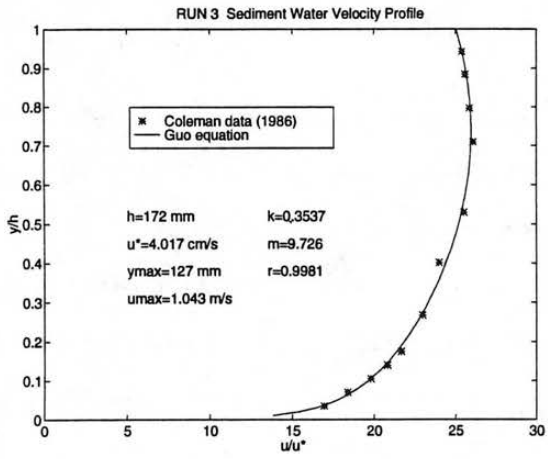
RUN 3 Sediment Water Velocity Profile
Coleman data (1986)
Guo equation
h=172 mm
k=0.3537
u*=4.017 cm/s
m=9.726
ymax=127 mm
r=0.9981
umax=1.043 m/s
y/h
u/u*

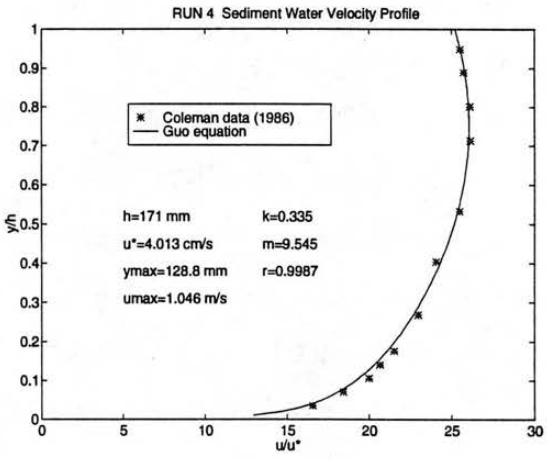
RUN 4 Sediment Water Velocity Profile
Coleman data (1986)
Guo equation
h=171 mm
k=0.335
u*=4.013 cm/s
m=9.545
ymax=128.8 mm
r=0.9987
umax=1.046 m/s
y/h
u/u*

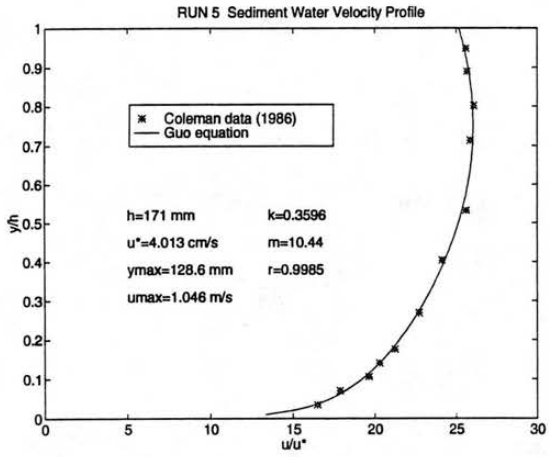
RUN 5 Sediment Water Velocity Profile
Coleman data (1986)
Guo equation
h=171 mm
k=0.3596
u*=4.013 cm/s
m=10.44
ymax=128.6 mm
r=0.9985
umax=1.046 m/s
y/h
u/u*

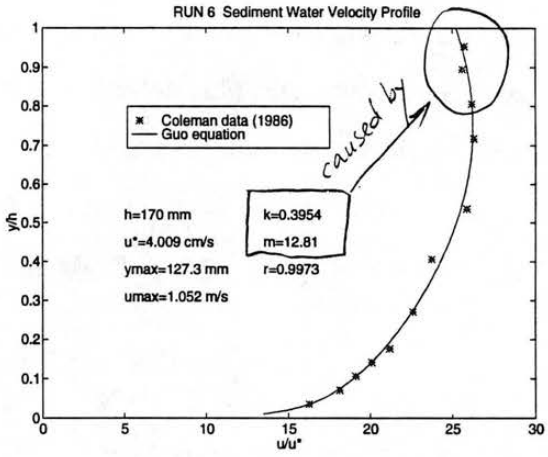
RUN 6 Sediment Water Velocity Profile
Coleman data (1986)
Guo equation
caused by
h=170 mm
k=0.3954
u*=4.009 cm/s
m=12.81
ymax=127.3 mm
r=0.9973
umax=1.052 m/s
y/h
u/u*

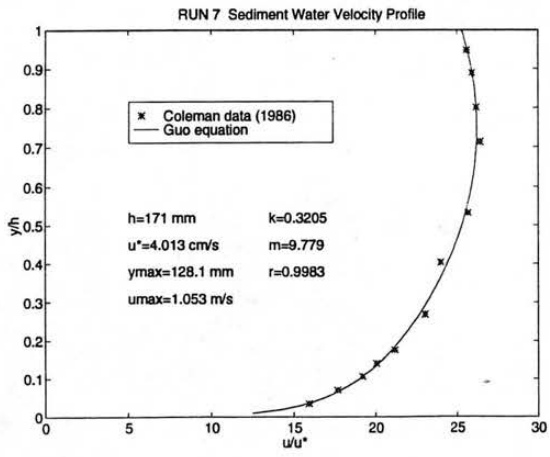
RUN 7 Sediment Water Velocity Profile
Coleman data (1986)
Guo equation
h=171 mm
k=0.3205
u*=4.013 cm/s
m=9.779
ymax=128.1 mm
r=0.9983
umax=1.053 m/s
y/h
u/u*

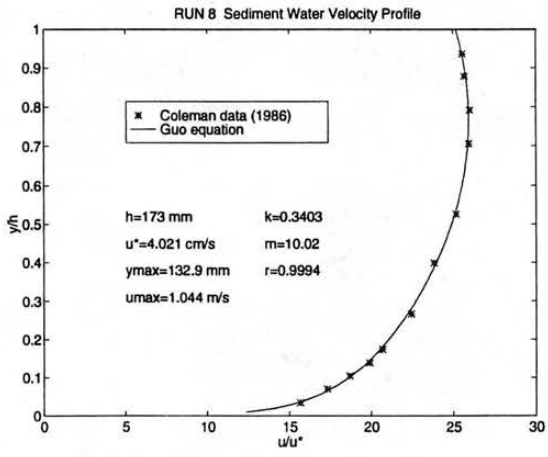
RUN 8 Sediment Water Velocity Profile
Coleman data (1986)
Guo equation
h=173 mm
k=0.3403
u*=4.021 cm/s
m=10.02
ymax=132.9 mm
r=0.9994
umax=1.044 m/s
y/h
u/u*

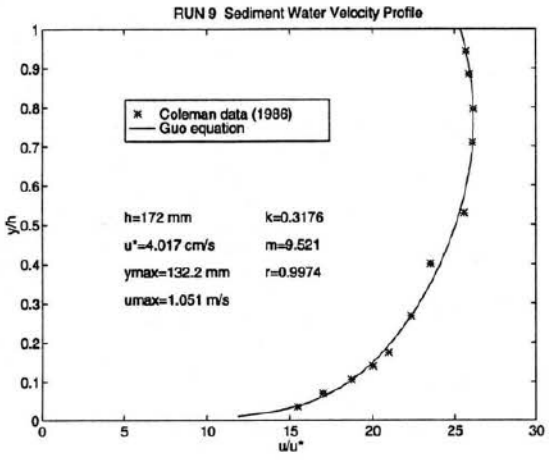
RUN 9 Sediment Water Velocity Profile
Coleman data (1986)
Guo equation
h=172 mm
k=0.3176
u*=4.017 cm/s
m=9.521
ymax=132.2 mm
r=0.9974
umax=1.051 m/s
y/h
u/u*

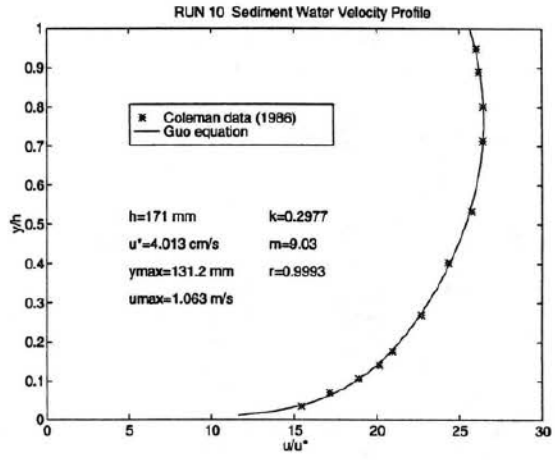
RUN 10 Sediment Water Velocity Profile
Coleman data (1986)
Guo equation
h=171 mm
k=0.2977
u*=4.013 cm/s
m=9.03
ymax=131.2 mm
r=0.9993
umax=1.063 m/s
y/h
u/u*

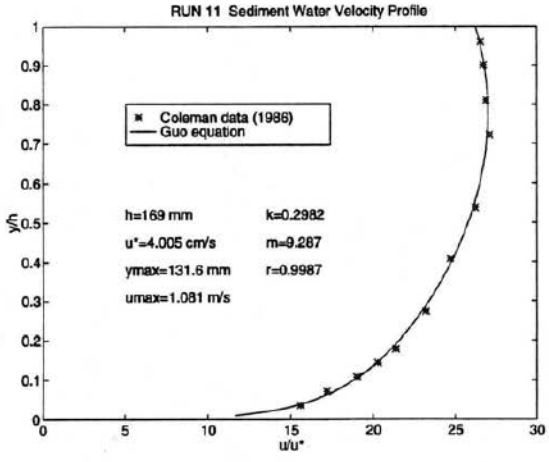
RUN 11 Sediment Water Velocity Profile
Coleman data (1986)
Guo equation
h=169 mm
k=0.2982
u*=4.005 cm/s
m=9.287
ymax=131.6 mm
r=0.9987
umax=1.081 m/s
y/h
u/u*

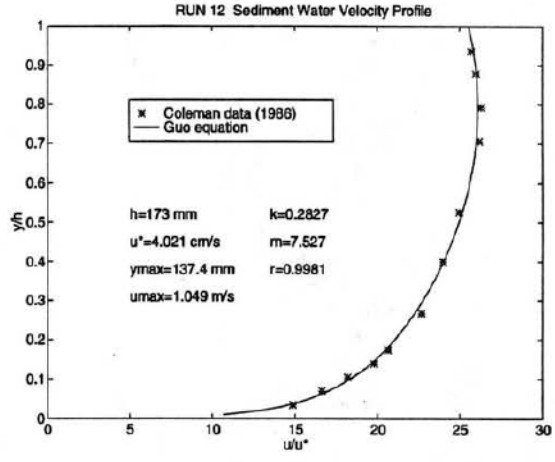
RUN 12 Sediment Water Velocity Profile
Coleman data (1986)
Guo equation
h=173 mm
k=0.2827
u*=4.021 cm/s
m=7.527
ymax=137.4 mm
r=0.9981
umax=1.049 m/s
y/h
u/u*

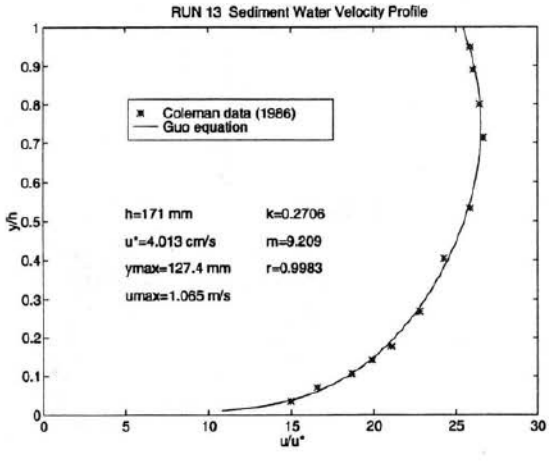
RUN 13 Sediment Water Velocity Profile
Coleman data (1986)
Guo equation
h=171 mm
k=0.2706
u*=4.013 cm/s
m=9.209
ymax=127.4 mm
r=0.9983
umax=1.065 m/s
y/h
u/u*

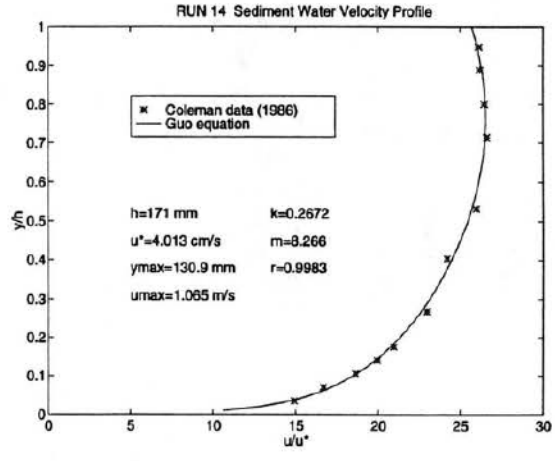
RUN 14 Sediment Water Velocity Profile
Coleman data (1986)
Guo equation
h=171 mm
k=0.2672
u*=4.013 cm/s
m=8.266
ymax=130.9 mm
r=0.9983
umax=1.065 m/s
y/h
u/u*

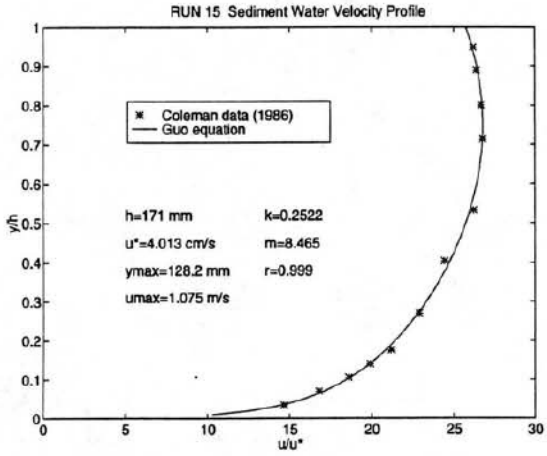
RUN 15 Sediment Water Velocity Profile
Coleman data (1986)
Guo equation
h=171 mm
k=0.2522
u*=4.013 cm/s
m=8.465
ymax=128.2 mm
r=0.999
umax=1.075 m/s
y/h
u/u*

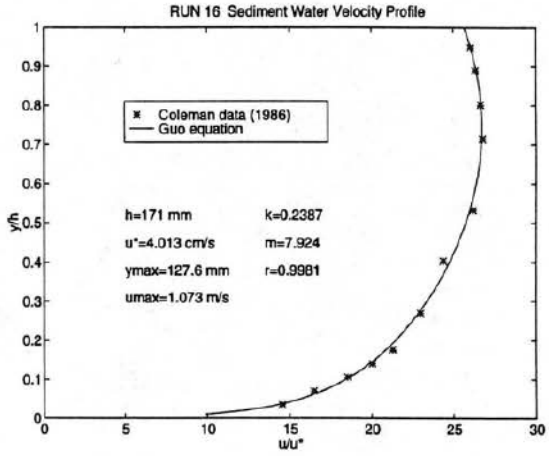
RUN 16 Sediment Water Velocity Profile
Coleman data (1986)
Guo equation
h=171 mm
k=0.2387
u*=4.013 cm/s
m=7.924
ymax=127.6 mm
r=0.9981
umax=1.073 m/s
y/h
u/u*

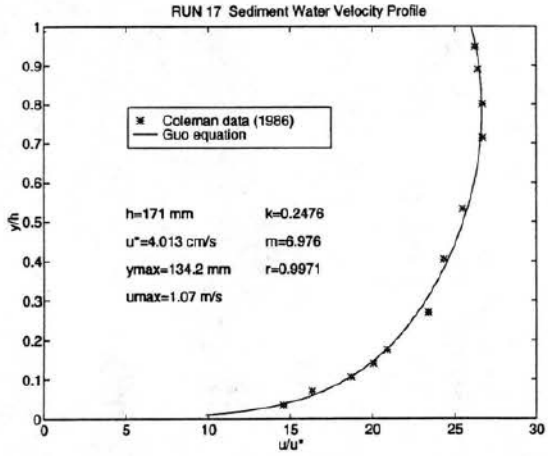
RUN 17 Sediment Water Velocity Profile
Coleman data (1986)
Guo equation
h=171 mm
k=0.2476
u*=4.013 cm/s
m=6.976
ymax=134.2 mm
r=0.9971
umax=1.07 m/s
y/h
u/u*

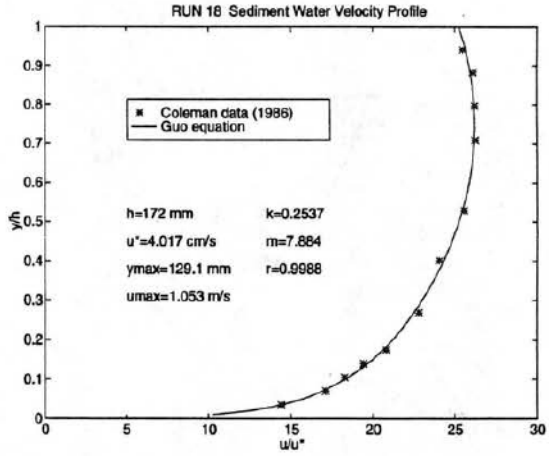
RUN 18 Sediment Water Velocity Profile
Coleman data (1986)
Guo equation
h=172 mm
k=0.2537
u*=4.017 cm/s
m=7.884
ymax=129.1 mm
r=0.9988
umax=1.053 m/s
y/h
u/u*

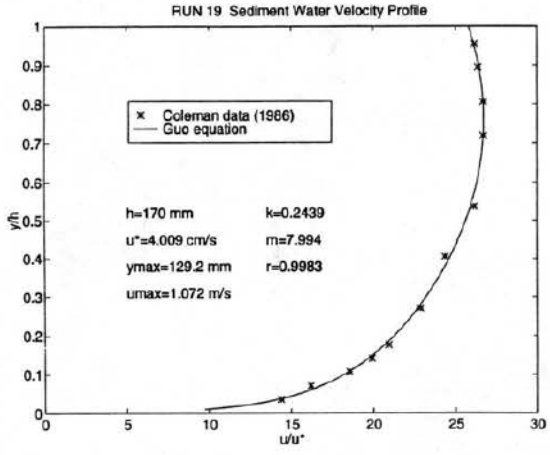
RUN 19 Sediment Water Velocity Profile
Coleman data (1986)
Guo equation
h=170 mm
k=0.2439
u*=4.009 cm/s
m=7.994
ymax=129.2 mm
r=0.9983
umax=1.072 m/s
y/h
u/u*

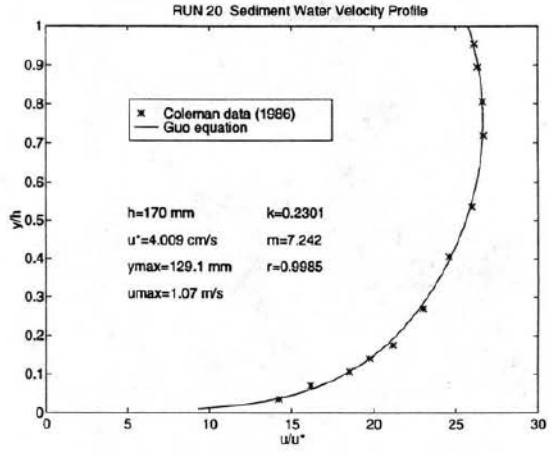
RUN 20 Sediment Water Velocity Profile
Coleman data (1986)
Guo equation
h=170 mm
k=0.2301
u*=4.009 cm/s
m=7.242
ymax=129.1 mm
r=0.9985
umax=1.07 m/s
y/h
u/u*

IV. RESULTS AND CONCLUSIONS

From Figures 1-20, it can be seen that: (1) The theoretical velocity profile equation fits the experimental data very well in the main flow region; (2) the model is valid even the maximum velocity occurs under water surfaces; (3) the presence of sediment concentration clearly makes the Karman constant κ decrease; (4) the mixing length strength m seems not very sensitive to the concentration, it varies in a small range of 7-10 except RUN 6, where the data near surface seems incorrect; (5) the parameter m in this model has the same role of the parameter Π in the log-wake law, which is an outer region variable and independent of the inner variables, such as viscosity; and (6) the conclusions confirm the Einstein and Chien's argument, i.e., the Karman constant κ decreases for sediment-laden flows. It is interesting to note that the conclusions ~~which~~ drawn from Coleman's data are against the Coleman's opinion. This may be caused by using different fitting methods.

V. APPENDIX: MATLAB CODE FOR VELOCITY PROFILE ANALYSES

A. Program: Velocity Profile Analyses (MATLAB Language)

```
%Note: Change run number and Err?.m
clear, hold off, load data.m
%Change the following parameter
run=1; %run number
n=6; %Sample number to determine ymax and umax
h=data(13,run+1); %Flow depth (mm)
%Determine the bed shear stress from Guo's formula
w=356; %Flume width (mm)
x=pi.*h./w; x1=atan(exp(-x));
x2=1./x.*(1.-exp(-0.62.*x)-0.62.*x.*exp(-0.62.*x));
Pb=4./pi.*(x1+x2); %bed shear Percentage of 2-D shear
ustar=sqrt(9.81.*h./1000.*0.002.*Pb); %Bed shear stress (Pa)
%Plot experimental profile
y0=data(1:12,1)./h; %Relative distance from bottom
```

```
u0=data(1:12,run+1)./ustar; %value of u/u*
plot(u0,y0,'*'), hold on
%Determine ymax and umax
y1=data(n:12,1)./h; u1=data(n:12,run+1)./ustar;
c=polyfit(y1,u1,2); a=c(1); b=c(2); cc=c(3);
ymax=-b./2./a; %The position of maximum velocity
umax=cc-a*ymax.^2; %The maximum velocity
%Nonlinear Optimizations of m and k
%Invoke function Err?.m
[mk out]=fmins('Err1',[10,0.4]); %Err1 is fmin function
m=mk(1); %The value of m
k=mk(2); %The value of k
%Plot the theoretical profile
y=0.01:0.01:1; %Relative distance from bottom
u1=(ymax-y).^2; u2=2.*(1.-y).*(ymax-y)./m.*log(1.-(1.-y).^m);
u=umax-m/2/k.*(u1-u2); %The value of theoretical velocity u/u*
plot(u,y), %Plot theoretical profile
%Calculate the associated coefficient r
y=data(1:12,1)./h; u1=(ymax-y).^2;
u2=2.*(1.-y).*(ymax-y)./m(1).*log(1.-(1.-y).^m(1));
u3=umax-m./2./k.*(u1-u2); %value corresponding to samples
c=corrcoef(u0,u3); r=c(1,2); %The value of associated coefficient
%Annotation
axis([0 30 0 1]), xlabel('u/u*'), ylabel('y/h'),
title(['RUN ',num2str(run),' Sediment Water Velocity Profile'])
text(5,0.52,['h=',num2str(h),' mm']), text(13.5,0.52,['k=',num2str(k)]),
text(5,0.38,['ymax=',num2str(ymax*h),' mm']),
text(5,0.31,['umax=',num2str(umax*ustar),' m/s']),
text(13.5,0.45,['m=',num2str(m)]),
text(5,0.45,['u*=',num2str(ustar*100),' cm/s']),
```

```
text(13.5,0.38,['r=',num2str(r)]),
legend('Coleman data (1986)','Guo equation')
```

B. **Subprogram: Nonlinear Optimizations of m and k**

```
function Y=Err1(m)
%m=[m k]
ymax=.7709; %Change this line
umax=26.2437; %Change this line
ustar=0.0402; %Change this line
y=[6 12 18 24 30 46 69 91 122 137 152 162]'./172; %Change this line
u=[.709 .773 .823 .849 .884 .927 .981 1.026 ... %Change this line
1.054 1.053 1.048 1.039]'./ustar; %Change
f1=(ymax-y).^2; f2=2.*(1-y).*(ymax-y)./m(1).*log(1-(1-y).^m(1));
f=umax-m(1)./2./m(2).*(f1-f2); Y=(1-f./u)'*(1-f./u);
```

VI. REFERENCES

Coleman, N. L. (1981). "Velocity profiles with suspended sediment," J. Hydraulic Research, 19(3), 211-229.

Coleman, N. L. (1988). "Effects of suspended sediment on the open-channel velocity distribution," Water Resources research, 22(10), 1377-1384.

Coles, D. (1956). "The law of the wake in the turbulent boundary layer," J. Fluid mechanics, 1, 191-226.

Einstein, H. A. and Chien N. (1955). "Effects of heavy sediment concentration near the bed on velocity and sediment distribution," Rep. 8, University of California, Berkley, and Missouri River Div., U. S. Army Corp. of Engineers.

Guo, Junke (1988). "Vertical distributions of velocity and sediment concentration in wide open channel," J. Taiyuan University of Technology, 19(2) 17-24.

Julien, P. Y. (1995). Erosion and Sedimentation. Chapter 6, Cambridge University Press.

Lyn, D. A. (1988). "A similarity approach to turbulent sediment-laden flows in open channels," J. Fluid Mechanics, (193), 1-26.

Vanoni, V. A. (1946). "Transportation of suspended sediment by water," Tans. ASCE, (3)67-133.

Concepts of Design and Practice for Irrigation System in Sudan

Eldaw, Ahmed Khalid

Abstract

Design methods and methodologies were developed over years. The design of stable canals in Sudan is based on regime formulas. These formulas are valid for conditions prevailing before the construction of the Roseires and Sennar reservoirs, and before the dry years that changed the sediment concentrations in the canals. The local rainfall reduction also cause irrigating during the flood season(high sediment concentrations). The design adopted by old regime equations is not satisfactory and a new design concept for the new regime is necessary. In this short study two methods of designing an alluvial channels were used. The methods used were the regime theory and the downstream geometry approach developed by Julien and Waragadalam (1995), refer to hereafter as the downstream geometry approach. The results were based on field data and model data. In some cases the two methods were compared. Data used were from international rivers and channels, some were man-made canals and models.

Literature review:

The design of stable channels is a subject which has received attention from many investigators. The stable alluvial canals are characterized by a mobile bed which neither silts nor scours, Chang (1985). When such canals are connected within a system, their widths, depths, and slopes must be properly related under the specific distributions in water discharge and sediment load in order to maintain the approximate equilibrium or regime. The methods for designing stable channels may be generally categorized as belonging to one of the following design criteria: (1) Maximum permissible velocity; (2) tractive force; (3) regime theory. Channels are said to be in regime when scour and deposition occur, but the balance of these is such that the boundaries remain essentially in equilibrium over a period of time, McKiernan (1993). In this condition the materials transported by the flow and forming the boundaries are of similar origin and accordingly have generally the same physical characteristics. Simons and Albertson (1960) studied the relationship between the regime theory and the limiting tractive force theory, they described the possibility of combining the strong points of the two systems.

Empirical regime formulas have been developed by several investigators, notably Lacey (1936), Simons and Albertson (1960). Successes have also been made to rationalize the stable canal geometry by bringing out the underlying mechanics, Gill (1980) and to relate regime equations for the depth to flow resistance theories, Chang (1980) and Haynie and Simons (1968), channel slope to sediment transport mechanics, Chang (1980) and White et al (1982) and the width to minimum stream power, Chang (1980) or maximum sediment efficiency, White et al (1982). Mahmood and Shin (1971), presents and summarize the various analyses of the developments of the "regime theory", this include, Kennedy's critical velocity equation, Lindley's enunciation of regime, Lacey's regime equations and the Irrigation Research Institute Equations.

The Ministry of irrigation and water resources (Sudan) has established hydraulic design procedures for the standardized canals and hydraulic structures which are published as "design sheets" series. The Manning's formula was used for the determination of the waterway section and the velocity for all canals. The coefficient of roughness, "n" was taken to be 0.025. The recommended maximum permissible velocity of water for the clay soils was taken as 0.60 to 0.90 m/s and 0.30 to 0.60 m/s for very light loose to average sandy soils. For the determination of the water slope the Lacey regime equations are used. Lacey's method was the accepted procedure for the hydraulic design of canals in the Sudan Gezira irrigation scheme and the same adopted for design other canals with slight modification with respect to the silt factor and the adopted Manning's n. In future, detailed data collection and research on the Sudan irrigation canals should be oriented towards the explanation and improvement of the sediment transport relation in the Sudan canals. A joint study between the Hydraulic research Station (HRS-MOI-Sudan) and the Hydraulic Research Limited (HRL-Wallingford-UK), deals with silt management, should encounter the design criteria. The study computed 11% of the silt deposited in the main canals, 23% in the branches and the major canals 33% in the minor canals and about 33% of the amount of silt entering the Gezira Scheme deposited on the field. The diversification and the intensification experience in Gezira highlights the need for improvements and revision for the design criteria. Also the relatively dry years on the watershed , the high silt concentration due to the fact that the dead storage in reservoirs occupied by silts, and the low quality maintenance process make the situation even more difficult.

Sine the introduction of Lacey's regime equations basically no further development in alluvial canal design have been applied or adopted in Pakistan, Baker et al (1985). Bakker et al (1989), analyzed extensive data to develop a new design procedure for alluvial canals in Pakistan, sediment transport considerations form an integrated part of the new design procedure. Their study comprises an improved Lacey's width prediction and a modified van Rijn velocity predictor.

The data for this study is obtained from Sudan, Ahmed (1992) and Ahmed and Saad (1992), for Egypt from Ahmed and Saad (1992), data from Pakistan and United State of America from Simons and Albertson (1960) and Haynie and Simons (1968). Data for rivers from USA, India, and Switzerland was obtained from Blench and Qureshi (1964).

Gezira canal system design

The irrigation system of the Gezira Scheme starts with the twin main canals from the head regulator at Sennar dam with capacities of 186 m^3/s and 168 m^3/s which run northward along a main ridge for nearly 57 km. From this point the Gezira main canal continues for a further distance of nearly 145 km. Branch canals and a large number of major and minor canals branch off to serve the irrigated area. The main canal reaches vary in length from 6 to 22 km. These reaches are controlled by cross regulators maintaining upstream pools of constant levels to enable branches and majors to draw the required amount of water. The major canals are divided into reaches of about 3 km in length by cross regulators. The minor canals and/or lateral canals are grouped at these points and measured discharges are passed through them. Minor canals are provided with intermediate regulators in the form of storage weirs. The function of these structures is to pass the water needed for irrigation by day and to enable the storage of the night flow, which is not passed to the field until the next day, in the different reaches of the minor canals.

The Ministry of Irrigation and Water Resources (MOI) has established hydraulic design procedures for the standardized canals and hydraulic structures which are published as the "design sheets". Main canals and branches are designed to have a maximum command of 2.0 m at the upstream pool of the intermediate regulators where major canals takeoff. The water surface slopes are generally limited to 7-9 cm/km. However, it is preferable that the slope of the reach under design is made as close as possible to the Lacey slope for a silt factor of 0.63. The free board is 1.0 m and the berm width is 2.0 m. For major canal and pump channels the maximum command is limited to 0.8 m. And it should at the same time be sufficient to guarantee the passage of the designed discharges of the minor canals and the watercourses. It should also be 0.50 m above upstream pool level of the next cross regulator to provide an adequate water slope of about 10 cms per km and sufficient head of 0.25 on the regulator, The free board is limited 0.75 m and the berm width is 0.50 m.

Regime theory

Regime formulas for canals in the most general form were given as functions of the discharge as follows:

$$B = C_d Q^{\alpha} \quad \text{.....(1)}$$

$$S = C_s Q^{\eta} \quad \text{.....(2)}$$

$$V = C_v Q^{\gamma} \quad \text{.....(3)}$$

$$h = C_d Q^{\beta} \quad \text{.....(4)}$$

The coefficients and the exponents are constant for any particular conditions. For continuity consideration:

$$\alpha + \beta + \gamma = 1 \quad \text{.....(5)}$$

A little reflection from the reviewed data will show that it is not possible to co-ordinate formulas of this type since both exponent and coefficients vary. Lacey (1931) substituted the depth by the hydraulic radius and introduced a silt factor "f" as:

$$S = 382.6 * 10^{-6} f^{1.5} R^{-0.5} \quad \text{.....(6)}$$

The Gezira canalization system was designed using the regime theory. For the determination

$$P = 4.84 Q^{0.5} \quad \text{.....(7)}$$

$$S = 14.3 Q^{-0.17} \quad \text{.....(8)}$$

$$A = 2.64 Q^{0.83} \quad \text{.....(9)}$$

of the water slope and some geometrical parameters, the Lacey regime equations in metric units as shown below were used:where P = wet perimeter of the water section (m); S = water slope in cm/km; Q = the discharge (m^3/s); and A = the flow cross-sectional are (m^2). Manning formula was used for the determination
of the waterway section and the velocity for all canals. The coefficient of roughness "n" was taken to be 0.025. The recommended maximum permissible velocity of water for fine soils was taken at 0.60 to 0.90 m/s and 0.30 to 0.60 m/s for very light loose to average sandy soils.

Downstream hydraulic geometry approach

Julien and Wargadalam (1993) proposed four theoretical hydraulic geometry relationships of alluvial channels as a function of three independent variables; discharge, mean particle diameter, and slope. In general their relationship can be written as follows:

$$dependent\ variable = f(Q, ds, S) \quad \text{.....(10)}$$

The dependent variables also was related to Q, ds and the shield parameter in the same study. The dependent variables obtained from this approach were the flow depth, h, the top flow width, W, and the average flow velocity, U, and the shield parameter. The relationships developed to obtain these dependent variables were as follows:

$$h = 0.2 Q^{\frac{2}{5+6m}} d_s^{\frac{6m}{5+6m}} S^{\frac{-1}{5+6m}} \quad \text{.....(11)}$$

$$W = 1.33Q^{\frac{2+4m}{5+6m}} d_s^{\frac{-4m}{5+6m}} S^{\frac{-1-2m}{5+6m}} \quad \text{.....(12)}$$

$$U = 3.76Q^{\frac{1+2m}{5+6m}} d_s^{\frac{-2m}{5+6m}} S^{\frac{2+2m}{5+6m}} \quad \text{.....(13)}$$

$$\iota_\Theta = 0.121Q^{\frac{2}{5+6m}} d_s^{\frac{-5}{5+6m}} S^{\frac{4+6m}{5+6m}} \quad \text{.....(14)}$$

Data

The data upon which this short study based was obtained from canal studies in Sudan, Egypt and the United States. The data taken in the field from the selected stable canals reaches included mainly, the magnitude of discharge, the average velocity, the slope, canals materials, depth, area, bed width and top width. It is worth mentioning that these information may not be complete for all canals. The data required to estimate the canal geometry and some hydraulics parameters were available for all canals. The sources of data were Simons and Albersons (1960), Hynie and Simons (1968), Blench and Qureshi (1964), Simons and Richardson (1962), Ahmed (1992), and Ahmed and Saad (1992). All the data were obtained as field data except that by Simons and Richardson, which was obtained from a physical model. The data from Blench and Qureshi (1964) were covered main rivers with very high flows and the rivers materials ranges from sand soils to course materials. Blench and Qureshi (1964) included data from rivers of USA, India and Switzerland.

Analysis of results

Table 1. showed that the downstream geometry approach highly overestimated the canal geometry, while the regime theory reasonably predict the canal geometry. This may be attributed to the degree of cohesiveness of the canal material. The Gezira irrigation canals ranges from clay to fine and medium sand. The portion of the canal under investigation is mainly composed of fine materials. The canal was originally designed by the regime theory, that is why the regime theory agreed well with the measured values. The downstream geometry approach produced a reasonable flow depth, very wide canal with low flow velocities. The low velocities and the large width compensate for high velocity and relatively narrower canal by the regime theory, so the continuity was satisfied by both methods.

Table 1. Comparison between the downstream geometry approach and the regime theory for canal geometry and hydraulics for the Gezira canals (Sudan)

	Q	ds	S	h	W	u	A	P	Rh
units	**m^3/s**	**mm**	**10^5**	**m**	**m**	**m/s**	**m^2**	**m**	**m**
DGA	**186**	**0.08**	**6.00**	**3.7**	**158**	**0.32**	**580**	**165**	**3.50**
DGA	**168**	**0.08**	**6.00**	**3.5**	**152**	**0.31**	**530**	**160**	**3.30**
Regim	**186**	**0.08**	**5.88**	**3.0**	**64**	**0.92**	**202**	**66**	**3.06**
Regim	**168**	**0.08**	**5.98**	**3.0**	**62**	**0.90**	**186**	**63**	**2.95**
Actual	**170**	**0.08**	**6.00**	**3.5**	**60**	**0.85**	**200**	**75**	**3.00**

Actual values were estimated from the experience of the writer on those canals. The parameters which are not computed directly from the theories were approximated using some relationships and judgement.

The canals geometry and the hydraulic factors computed by the downstream geometry approach showed a strong correlation with the observed. Though the two values may highly differ, particularly in the case of the man-made canals. The natural rivers obtained better values of the measured geometry and hydraulic factors. Figures 1 through 5, relates the geometric parameters and the hydraulic factors for the downstream geometry approach and the regime theory and the observed values. The downstream geometry approach overestimate the flow depth for smaller flow depths and underestimate the flow depth at relatively larger depths for the three canals (Tawfiky, Behery and Manoufy), Fig. 1. About 92% of the points lies between +6% and -7% of the best fitted line. The relationship obtained with correlation coefficient (r =0.906) as follows:

$$h = 1.956222 + 0.484374h \quad \text{.....(15)}$$

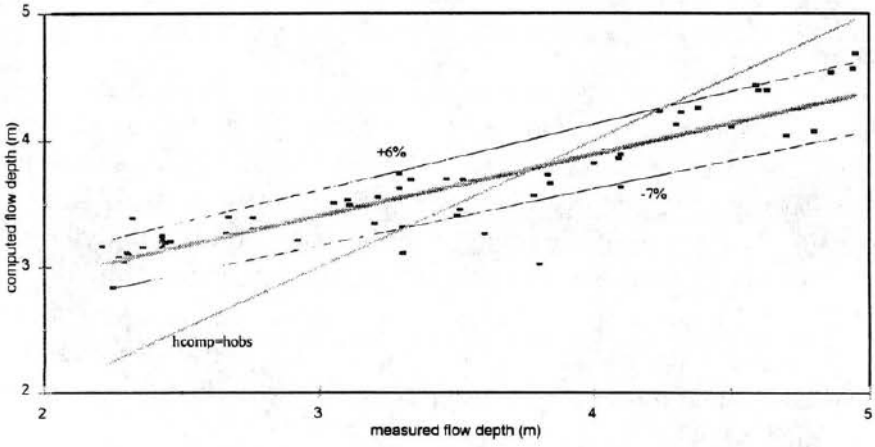

Fig. 1 Computed flow depth vs measured for Tawfiky, Behery and Manoufy canals

Figure 2 showed a high correlation of the velocity computed by downstream geometry approach and the observed. The correlation was as high as r=0.93 for Tawfiky and r=0.92 for Behery and Manoufy canals together. This may be due to the fact that later canals are wider and the former was relatively steeper. In comparison with the other two canals, Behery canal was much mild. The relationships developed for Tawfiky and Behery and Manoufy were respectively as follows:

$$U_{comp} = -0.04463 + 0.376417 U_{obs} \quad \text{.....(16)}$$

$$U_{comp} = 0.080824 + 0.362041 U_{obs} \quad \text{.....(17)}$$

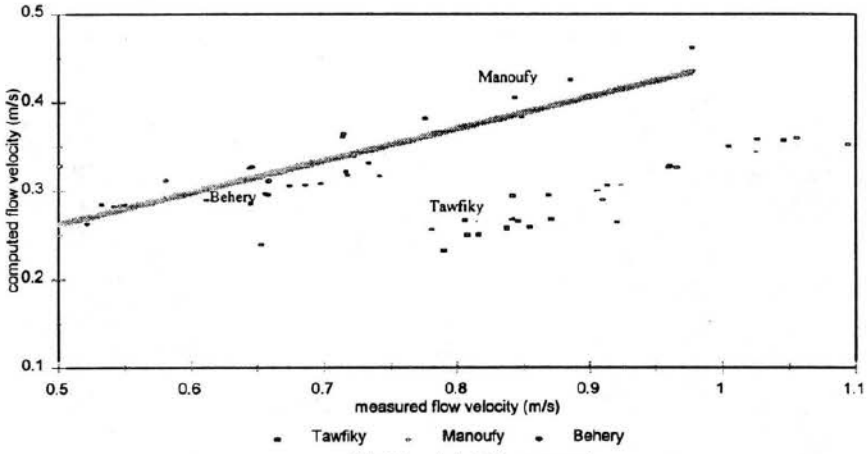

Fig. 2 Computed velocity vs measured for Tawfiky, Behery, and Manoufy canal

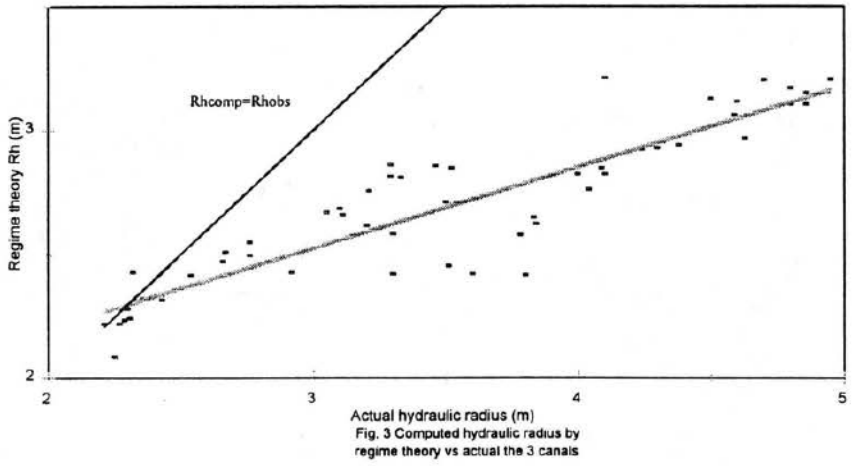

Fig. 3 Computed hydraulic radius by regime theory vs actual the 3 canals

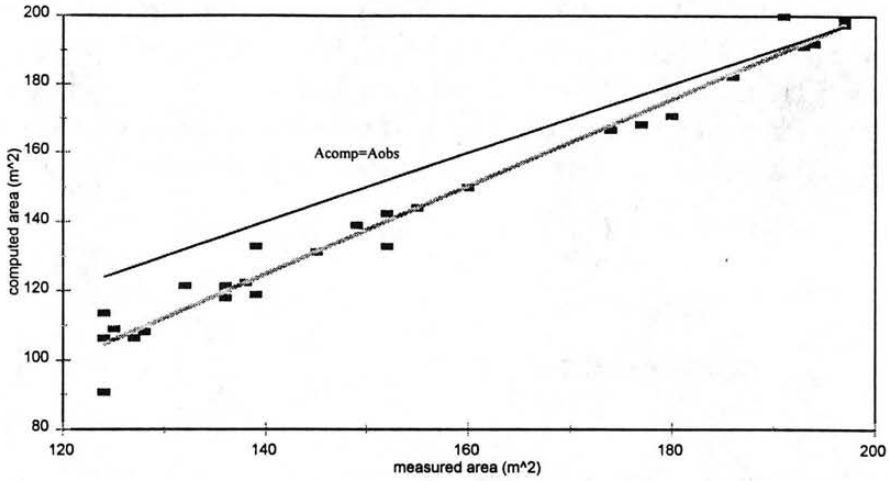

Fig. 4 Area computed by Regime theory for Tawfiky canal

Figure 3 shows the hydraulic radius computed by the regime theory (equation 18), for the 3 canals. The relationship was similar to the flow depth relationship, equation 15 and Fig. 1. This because the canals were relatively wide and the flow depth is approximately represent to the flow depth in this case. The correlation coefficient was r =0.92 and the relationship was as follows:

$$Rh = 0.4725\left(\frac{Q}{f}\right)^{1/3} \quad \text{.....(18)}$$

$$Rh_{comp} = 1.55 + 0.326 Rh_{obs} \quad \text{.....(19)}$$

The regime theory produced reasonably the cross-sectional area for Tawfiky canal, Fig. 4. This was obtained with a correlation coefficient of r=0.99. The relationship obtained, and the regime theory (with f = 0.94) used, were respectively as follows:

$$A_{comp} = -52.5473 + 1.268 A_{obs} \quad \text{.....(20)}$$

$$A = 1.26 Q^{5/6} f^{1/3} \quad \text{.....(21)}$$

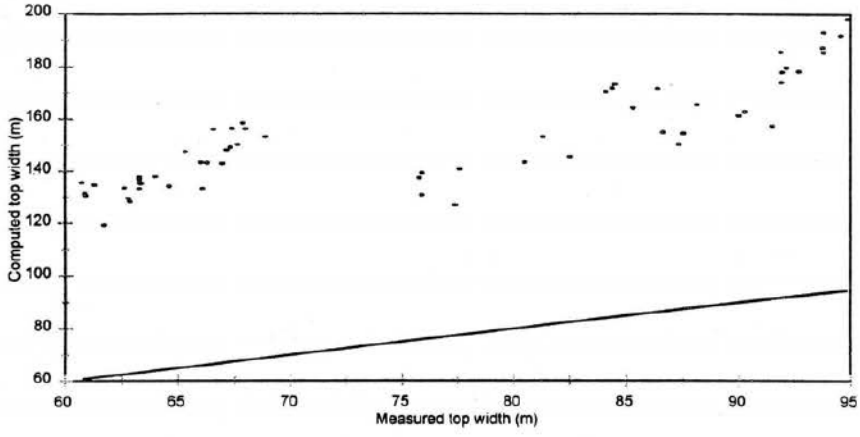

Fig. 5 Computed and predicted channel width for Tawfiky, Behery and Manoufy

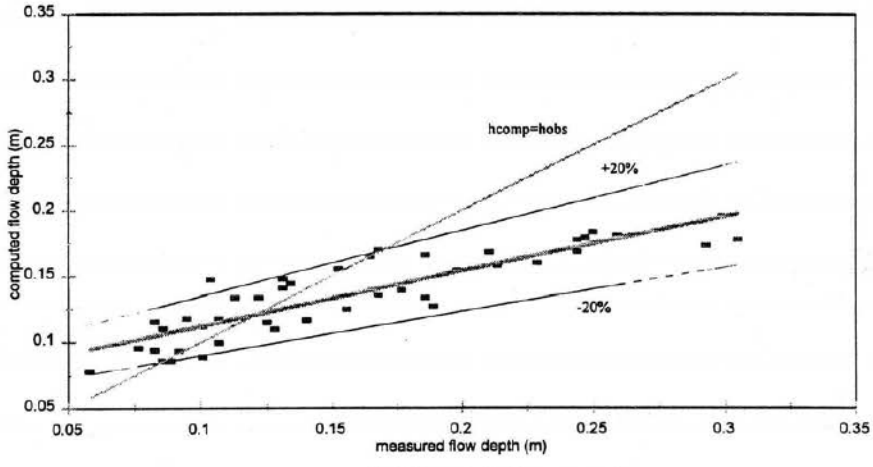

Fig. 6 Computed depth vs measured (1962)

Figure 5 the downstream geometry approach was clearly overestimate the top width. Figures 6 and 7 were developed from a model data. There was strong correlation between the flow depth and velocity computed by the downstream geometry approach and the measured flow depths and velocities. A correlation coefficients obtained for the flow depths and velocities were, r=0.885 and r=0.943, respectively. The relationships obtained were as follows:

$$h_{comp} = 0.0705 + 0.41673 h_{obs} \quad \text{.....(22)}$$

$$U_{comp} = 0.094 + 0.34108 U_{obs} \quad \text{.....(23)}$$

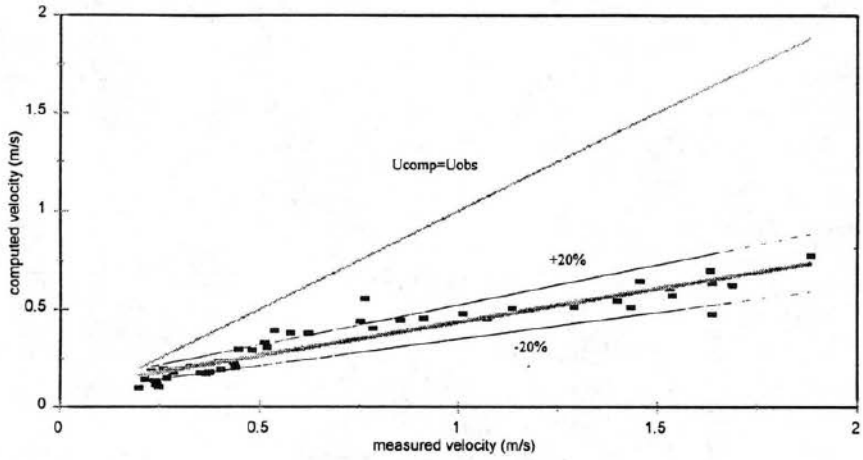

Fig. 7 Velocity computed vs measured (1962)

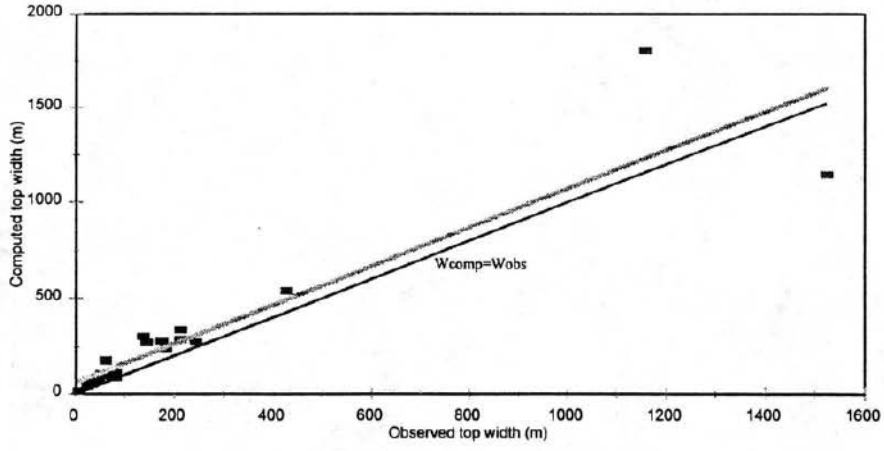

Fig. 8 Computed and measured top width of Rivers (Blench and Qureshi 1964)

Figure 8 was obtained from many natural rivers including the Mississippi river and others from India, Switzerland and USA. The downstream geometry approach produced a high correlation (r =0.92) between the computed and observed values of the top width. This indicates that the downstream geometry approach works well with natural canals with noncohesive materials. The relationship developed was as follows:

$$W_{comp} = 59.836 + 1.013 W_{obs} \quad \text{.....(24)}$$

Conclusion

The applicability of the regime theory and the downstream geometry approach has been emphasized in this paper by analyzing the available collected data on many canals and natural rivers in Sudan, Egypt, India, Switzerland and USA. Two basically different theories are used in this study because of the popularity of the regime theory and to study on the existing systems and to compare the newly developed downstream approach with the regime theory. The regime method is an empirical method which relies on available data and attempts to determine appropriate relationships from the data. The usefulness of this method depends on the quality of the data and the validity of the assumed form of the relationships. It has always been acknowledged that the various coefficients derived may not be truly constant but vary slightly and that the equations should only be applied in situations similar to those for which the data were collected. However, it is difficult to determine the degree of similarity and some criteria should be followed. Coefficients and exponents in the foregoing equations were found to vary depending on the river data used; no unique relationship has been determined.

Because of the less significant correlation between the downstream geometry approach estimation of flow velocity, top width, and flow depth as depicted by table 1, it was clear that within the cohesive range of particles other relations of the regime type are perhaps superior to the downstream geometry approach for estimating the design parameters. The downstream geometry approach method has providing a means for defining the channel geometry and hydraulic factors for natural rivers. This approach was based upon three independents. For a given water discharge, slope, and material size it may be applied to obtain the width, depth and flow velocity of channels regime. The concept employed herein implies that the width, depth and flow velocity of regime channel are governed by the given water discharge, slope and the medium particle size .

If one accepts the basic concepts presented herein, the following conclusions may be outlined for alluvial channel:

1. The regime theory developed by Kennedy, Lacey's and later modified by many investigators are only valid for limited range of conditions upon which they are based i.e. similar conditions
2. The regime theory always reproduces a constant slope.
3. The downstream geometry approach work well with natural channel compared with the man-made design channels. However, even for the there was strong correlation for the geometry and hydraulic factors between the computed and measured data.
4. The downstream geometry approach works better for non-cohesive material.
5. The downstream geometry approach reasonably estimated flow depth for all channels, overestimated the channel width, and underestimated the flow velocity, but never violated the continuity condition.
6. In all the cases the downstream geometry approach could be calibrated for any particular site and used for the design.
7. The downstream geometry approach allow the change in the slope.

References

Ahmed, S. E. (1992). "Alluvial canal adequacy." J. Irrig. Drain., ASCE, 118(4), 543-554.

Ahmed, S. E., and Saad, M. B. (1992). "Prediction of natural channel hydraulic roughness." J. Irrig. Drain., ASCE, 118(4), 632-639.

Blench, T., and Qureshi, M. A. (1964). "Practical regime analysis of river slope." J. Hydr. Div., ASCE, 90(HY2), 81-98.

Bakker, B., Vermaas, H., and Choudri, A. M. (1989). "Regime theories updated or outdated." Delft Hydraulics Laboratory, the Netherlands, 1-20.

Chang, H. H. (1979). "Geometry of rivers in regime." J. Hydr. Div., ASCE, 105(5), 691-706.

Chang, H. H. (1985). "Design of stable alluvial canals in a system." J. Irrig. Drain., ASCE, 111(1), 36-37.

Chang, H. H. (1980). "Stable alluvial canal design." J. Hydr. Div., ASCE, 106(5), 873-891.

Gill, M. A. (1968). "Rationalization of Lacey's regime flow equations." J. Hydr. Div., ASCE, 94(4), 983-995.

Haynie, R. B., and Simons, D. B. (1968). "Design of stable channels and alluvial materials." J. Hydr. Div., ASCE, 94(6), 1399-1420.

Lacey, G. (1936). "Note on regime diagrams for the design of canals and distributaries."

Julien, P. Y., and Wargadalam, J. (1995). "Alluvial channel geometry: theory and applications." J. Hydr. Div., ASCE, 121(4), 312-325.

Mahmoud, K., and Shen, H. W. (1971). "The regime concept of sediment-transporting canals and rivers." River mechanics, edited and published by: Shen, H. W., Vol. II, chap. 30.

Simons, D. B., and Albertson, M. L. (1962). "Uniform water conveyance channels in alluvial material." ASCE, Transactions, Vol. 127, 927-1006.

Simons, D. B., and Richardson, E. V. (1960). "Resistance to flow in alluvial channels." J. Hydr. Div., ASCE, 86(5), 33-71.

White, W. R., Bettes, R., and Paris, E. (1982). "Analytical approach to river regime." J. Hydr. Div., ASCE, 108(10), 1179-1193.

Zipparro, V. J., and Hasen, H. "Davis handbook of applied hydraulics." McGraw-Hill, New York, 1993. "Regime canals." McKiernan, B. A., Chap. 6.

DOWNSTREAM HYDRAULIC GEOMETRY
RIO APURE CASE STUDY

By Peter Molnár [1]

ABSTRACT: Downstream hydraulic geometry is predicted for the Rio Apure using three methods - regime theory, exponent method, and Julien and Wargadalam method. The predicted values are then compared to observed data; and the applicability and performance of each model is discussed.

INTRODUCTION

Defining a stable geometry of alluvial channels has received considerable attention in the past, and still continues to do so. The downstream variation of channel width, depth, slope, and velocity is an important component in understanding the stability of natural rivers. In this report, I used three methods to determine the downstream hydraulic geometry of Rio Apure, a tropical river in Venezuela, and compared the results with observed channel properties. First a brief review of each of the methods is provided, then a description of the Rio Apure basin and river data is provided. Finally, each method is used to compute downstream hydraulic geometry, and these calculations are compared to observed data. Some conclusions on the performance and applicability of the methods are drawn in conclusion.

DOWNSTREAM HYDRAULIC GEOMETRY - A REVIEW

Water and sediment discharges are widely accepted to be the governing factors in determining channel geometry of alluvial channels. The problem is to predict how a channel adjusts its geometry (channel depth, width and slope) in the downstream direction in order to transmit a given discharge and sediment load. In the past this question has been tackled from two perspectives: the empirical approach; and the analytical approach.

The empirical approach is data dependent and generally calibrates simple empirical equations describing the variation of channel properties downstream, using observed data. The analytical approach attempts to include the fundamentals of hydraulics, and sediment transport into these equations. Clearly, this becomes a complicated task, and has not yet been solved to the satisfaction of all those concerned. A "quasi-analytical" approach is often taken, which combines the virtues of both perspectives. In this exercise I chose to compare two empirical methods - the regime theory and the exponent method, with a "quasi-analytical" approach of Julien and Wargadalam.

[1] Ph.D. Candidate, Department of Civil Engineering, Colorado State University; molnarp@lamar.colostate.edu.

Regime Theory

The Anglo-Indian school of engineers offered a practical approach of determining the geometry of sediment laden channels, known as the "regime theory". Derived initially for canals with steady flow and fine sediment load in India, the theory consists of a set of empirical equations which give the width, depth and slope of an approximately stable channel whose cross-sectional form is maintained by a local balance between erosion and deposition.

One of the most important contributions to the design of regime canals was that of Lacey. Lacey introduced the following system of empirical relationships that determine the velocity (U), wetted perimeter (P), channel cross-section area (A), and slope (S) as a function of discharge (Q) and a silt factor (f) in English units (Simons and Senturk, 1977):

$$\begin{aligned} U &= 0.794\, Q^{\frac{1}{6}} f^{\frac{1}{3}} \\ P &= \frac{8}{3} Q^{\frac{1}{2}} \\ A &= 1.26\, Q^{\frac{5}{6}} f^{-\frac{1}{3}} \\ S &= 0.00055\, f^{\frac{5}{3}} Q^{-\frac{1}{6}} \end{aligned} \qquad (1)$$

The silt factor f was determined from:

$$f = 1.59\, d_{50}^{\frac{1}{2}} \qquad (2)$$

Where d_{50} is in mm. Lacey's empirical regime equations, as well as other regime theory equations developed later, were based on a fairly narrow range of sediment sizes and derived for irrigation canals with very low slope. Therefore, their application to natural rivers is restricted only to conditions for which they were originally intended.

The regime theory was a significant advance in an attempt to describe the stable channel geometry. Although strictly empirical in nature, it provided the basis for further research into channel equilibrium conditions. A nice discussion of the history and development of regime theory can be found in Wargadalam (1993).

Exponent Method

The variation of channel geometry as originally proposed by Leopold and Maddock (1953) was in a very simple form, and was a direct extension of the regime theory. Leopold and Maddock were the first to make a clear distinction between at-a-station and downstream hydraulic geometry. In the downstream direction they defined the following power laws that related channel width, mean depth and velocity to discharge of a given frequency of occurrence:

$$W = a\,Q^{b}$$
$$H = c\,Q^{f} \qquad (3)$$
$$U = k\,Q^{m}$$

From the data they analyzed, they found that the power law exponents did not vary greatly between basins, and the average values they found were b = 0.5, f = 0.4 and m = 0.1. Their analysis was conducted with respect to mean annual flow conditions, but also compared to flows of different frequencies.

Leopold and Maddock recognized that channel slope, bed roughness and sediment transport also play an intricate role in the geometry of channels, and affect the downstream hydraulic geometry, but they did not attempt to quantify this effect. The above "exponent method" with constant exponents has been used by many researchers as a basic indication of channel variation downstream.

Julien and Wargadalam Method

Julien and Wargadalam (1995) follow a physically based approach, in which they define the downstream hydraulic geometry relationships by solving four governing equations (continuity, resistance, secondary flow and particle mobility). They define channel width, depth, slope and average velocity as a function of discharge, sediment size, critical Shields parameter and streamline deviation angle. They calibrate and test their analytical expression using data from 835 field channels and 45 laboratory channels, covering a wide range of flow conditions. Their results have a wider range of applicability, and present a very sound physical approach to channel geometry.

Julien and Wargadalam present the following system of equations to determine the downstream hydraulic geometry of alluvial channels in terms of depth (H), width (W), average velocity (U), and the critical Shields parameter (τ^*), as a function of the independent variables - discharge (Q), sediment size (d_s), and slope (S), in metric units:

$$H = 0.2\,Q^{2/(5+6m)}\,d_s^{6m/(5+6m)}\,S^{-1/(5+6m)}$$
$$W = 1.33\,Q^{(2+4m)/(5+6m)}\,d_s^{-4m/(5+6m)}\,S^{-(1+2m)/(5+6m)}$$
$$U = 3.76\,Q^{(1+2m)/(5+6m)}\,d_s^{-2m/(5+6m)}\,S^{(2+2m)/(5+6m)} \qquad (4)$$
$$\tau^* = 0.121\,Q^{2/(5+6m)}\,d_s^{-5/(5+6m)}\,S^{(4+6m)/(5+6m)}$$

Where m is the exponent of the resistance equation and is a function of the relative submergence H/d_s. The calibration, verification, and validation of this system of equations can be found in Wargadalam (1993).

The innovative aspect of this study was that the authors included concepts of secondary flows in curved channels, and the three-dimensional mobility of noncohesive particles.

Other Research in Downstream Channel Geometry

Rhoads (1991) attempted to examine the variation in the coefficients and exponents of the downstream hydraulic geometry relationships by using a continuously varying parameter model. He took streamflow and various channel sediment characteristics to be the independent driving variables, and performed multiple regression analyses between all combinations of these variables and the depth and width of individual channel cross-sections. Using this statistical, empirical, approach he got expressions that relate individual coefficients and exponents of the hydraulic geometry relationships to various flow and sediment conditions.

Kolberg and Howard (1995) expand on the variable exponent model. They show the importance of channel bed material in determining the hydraulic geometry exponents. They also address the issue of whether it is appropriate to divide width versus discharge data into classes by their width:depth ratios.

RIO APURE, VENEZUELA

Rio Apure is a large alluvial river in Venezuela. It drains an area of 145 thousand km^2 and is a tributary of the Orinoco River (Fig. 1). The physiographical and geological features of the basin, together with the regional climate, provide a very distinct runoff pattern. The rainy season lasts from May through September, with August being on average the wettest month of the year. Rio Apure is formed by the confluence of the Sarare and Uribante Rivers. From there it flows about 670 km eastward, to join the Orinoco River. Its average annual contribution to the Orinoco is about 1950 m^3/s.

Rio Apure can be divided into three sections with different characteristics (Smith and Nordin, 1988). Reach 1, from Km 668.3 to Km 315.8, may be classified as sinuous braided, and is not very stable. Reach 2, from Km 315.8 to Km 210.1, the channel becomes narrower, less steep, and more sinuous. In Reach 3, from Km 210.1 to the confluence with Orinoco, an irregular meander pattern persists, with very low slope. Bed material consists of fine to medium sand.

In this study I used observations on the Rio Apure made by Mark Smith in preparation for his M.Sc. Degree and reported in Smith and Nordin (1988). All discharge, bed material, and channel cross-section observations for the 7 main gaging stations were done during a field experiment in June 1987 (a high flow month which corresponded to about the 2 year flood conditions) and are shown in Table 1.

STATION	River kilometer [km]	Channel width [m]	Channel area [m^2]	Mean depth [m]	Discharge [m^3/s]	Velocity [m/s]	Estimated channel slope [%]	Bed material d_{50} [mm]
Puente Remolino	668.3	175	576.0	3.29	688.2	1.2	0.0265	0.30
Palmarito	569.9	162	613.8	3.79	750.5	1.2	0.0216	0.28
Bruzual	443.6	272	906.4	3.33	1267.9	1.4	0.0166	0.29
El Saman	350.8	295	1259.4	4.27	1263.2	1.0	0.0136	0.40
Las Culatas	197.8	259	1491.4	5.76	1236.8	0.8	0.0099	0.35
San Fernando	182.0	564	2232.3	3.96	1691.9	0.8	0.0096	0.29
El Perro	10.1	273	1924.5	7.05	1303.8	0.7	0.0030	0.40

Table 1. Observations at 7 main gaging stations on Rio Apure (June 1987 experiment)

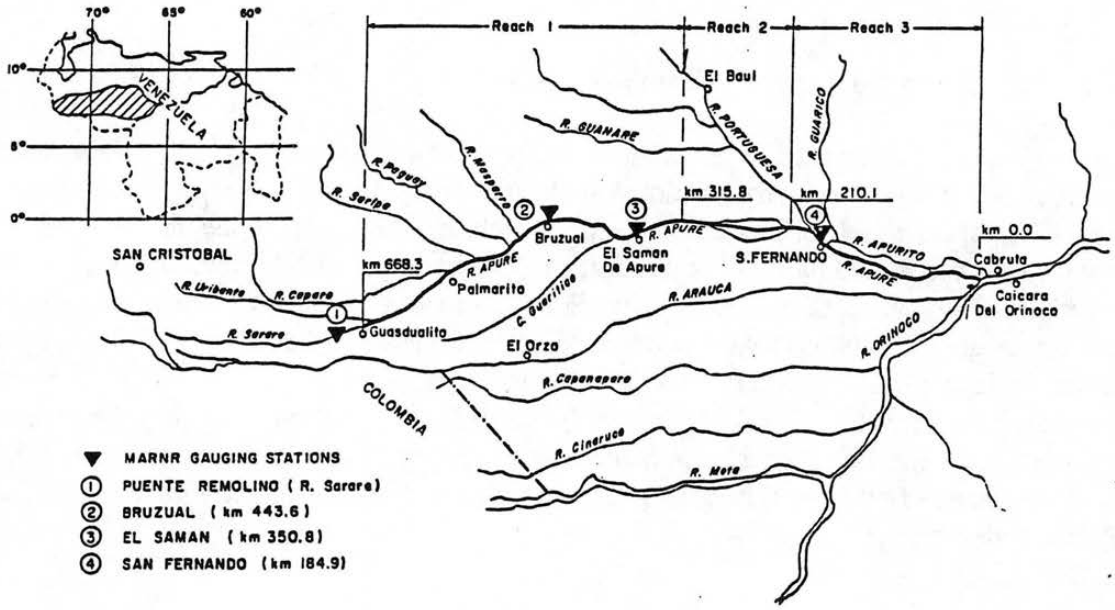

Figure 1. Rio Apure Basin schematic (Smith and Nordin, 1988).

RIO APURE - DOWNSTREAM HYDRAULIC GEOMETRY

The downstream hydraulic geometry of Rio Apure was determined using the three methods described earlier. The variation of average channel depth, width and velocity downstream was calculated as a function of observed discharge and bed material size at each station (where appropriate). The calculated values were then compared to observed average channel depth, width and velocity at each of the seven stations and evaluated.

Regime Theory

The regime theory equations required first to determine the silt factor from equation (2) using the observed d_{50} bed material size at each of the seven gaging stations (Tab. 1). Then the system of regime equations (1) was used to calculate the velocity (U), wetted perimeter (P), cross-section area (A) and slope (S) for each gaging station, given the silt factor and discharge (Tab. 1). The results are given in Table 2.

STATION	Silt factor f	U [m/s]	P [m]	A [m²]	S [%]	Width W [m]	Depth H [m]
Puente Remolino	0.871	1.244	126.71	553.53	0.00812	117.3	4.72
Palmarito	0.841	1.248	132.32	601.86	0.00755	122.5	4.91
Bruzual	0.856	1.369	171.99	926.26	0.00713	160.4	5.77
El Saman	1.006	1.444	171.67	875.21	0.00932	160.8	5.44
Las Culatas	0.941	1.407	169.87	879.30	0.00837	158.8	5.54
San Fernando	0.856	1.437	198.68	1177.99	0.00679	186.0	6.33
El Perro	1.006	1.452	174.41	898.59	0.00927	163.4	5.50

Table 2. Downstream hydraulic geometry for Rio Apure, calculated using the regime theory.

The top width and average depth of the channel at individual stations in Table 2 were determined from the cross-section area and wetted perimeter. Also note that the calculated slope of the channel is an order of magnitude greater than the observed slope in the upstream sections of the river, and does not decrease downstream in a consistent manner.

Exponent Method

The exponent method was used to develop long-term downstream hydraulic geometry relationships for Rio Apure of the form in equation (1). Based on available data for the period 1970-1972, the appropriate depth, width and velocity were plotted against average bankfull discharge at the 5 main gaging stations on the river to yield the following best fit (Smith and Nordin, 1988):

$$W = 0.65\ Q^{0.850}$$
$$H = 4.41\ Q^{0.013}$$
$$U = 0.35\ Q^{0.131}$$

Where Q is in m^3/s, W and H are in m and U is in m/s. From continuity, the parameters in equation (1) must satisfy the following: ack=1 and b+f+m=1. The best fit determined above yields: (0.65)(4.41)(0.35)=1.003 and 0.85+0.013+0.131=0.994, which is satisfactory. Also note that the fitted exponents b, f and m differ markedly from those found for rivers in the U.S. by Leopold and Maddock in their 1953 paper (b=0.5, f=0.4, and m=0.1). In Rio Apure, the downstream variation of width with discharge is considerably more pronounced than that of average depth.

Results from the above equations, using the discharge from Table 1 for each gaging station, are given in Table 3.

STATION	Calculated channel width W [m]	Calculated channel depth H [m]	Calculated average velocity U [m/s]
Puente Remolino	167.9	4.80	0.824
Palmarito	180.7	4.81	0.833
Bruzual	282.2	4.84	0.892
El Saman	281.3	4.84	0.892
Las Culatas	276.3	4.84	0.890
San Fernando	360.6	4.86	0.927
El Perro	288.9	4.84	0.896

Table 3. Downstream hydraulic geometry for Rio Apure, calculated using the exponent method.

Julien and Wargadalam Method

The system of equations (4) developed by Julien and Wargadalam (1995) was solved iteratively by selecting an initial resistance equation exponent *m*. Then, using the discharge, sediment size and slope data from Table 1, a channel depth H was calculated. The resistance exponent *m* was then recalculated using (Julien and Wargadalam, 1995):

$$m = \frac{1}{\ln \frac{12.2H}{d_s}} \tag{6}$$

This process was repeated until m did not change inbetween two calculation steps. The sediment size d_s was taken to be d_{50} for individual stations from Table 1. Discharge and slope values were also taken from Table 1 for each gaging station. The results of this analysis are presented in Table 4.

STATION	Channel depth H [m]	Channel width W [m]	Average velocity U [m/s]	Critical Shields par. τ^*
Puente Remolino	4.61	199.4	0.749	2.461
Palmarito	4.96	215.3	0.703	2.315
Bruzual	6.43	280.5	0.704	2.225
El Saman	6.78	288.6	0.646	1.394
Las Culatas	7.15	305.2	0.567	1.224
San Fernando	8.14	348.5	0.596	1.630
El Perro	9.23	396.0	0.355	0.421

Table 4. Downstream hydraulic geometry for Rio Apure, calculated using the Julien and Wargadalam method.

Different sediment sizes were also used in the analysis (d_{84}, d_{25}, d_{10}), but the results for the hydraulic geometry did not change significantly. Also note that the critical Shields parameter is well above incipient motion for the sediment sizes found on the river bed. Therefore, sediment transport in Rio Apure under the given conditions can be expected. This was also supported by observations, where measured sediment load decreased in the downstream direction (Smith and Nordin, 1988), as is suggested by the decrease in τ^* from the above simulations.

COMPARISON OF THE METHODS

Figures 2, 3 and 4 show plots of the calculated channel properties (depth, width and velocity) using the above methods versus the observed values. The comparison and discussion of these plots is done by "visual inspection", without statistical interpretation.

Channel width (Fig. 2) was predicted well by the exponent method and Julien and Wargadalam method. Regime theory underestimated the channel width. Also note that all methods underestimated the wide cross-section at San Fernando (564 m). One of the reasons for the worse performance of the regime theory model is that it does not use the observed slopes of the river sections in determining hydraulic geometry, but rather calculates the slope as a dependent variable on discharge and the silt factor. It describes a stable channel, and in this sense gives us an indication of what the Rio Apure downstream channel geometry should be under equilibrium conditions. The exponent method gives a very good fit to the observed width. This does not come as a surprise, since the parameters of the exponent method were calibrated for this particular channel and flow condition. The Julien and Wargadalam method overestimates the observed width slightly, but overall provides a fairly good fit.

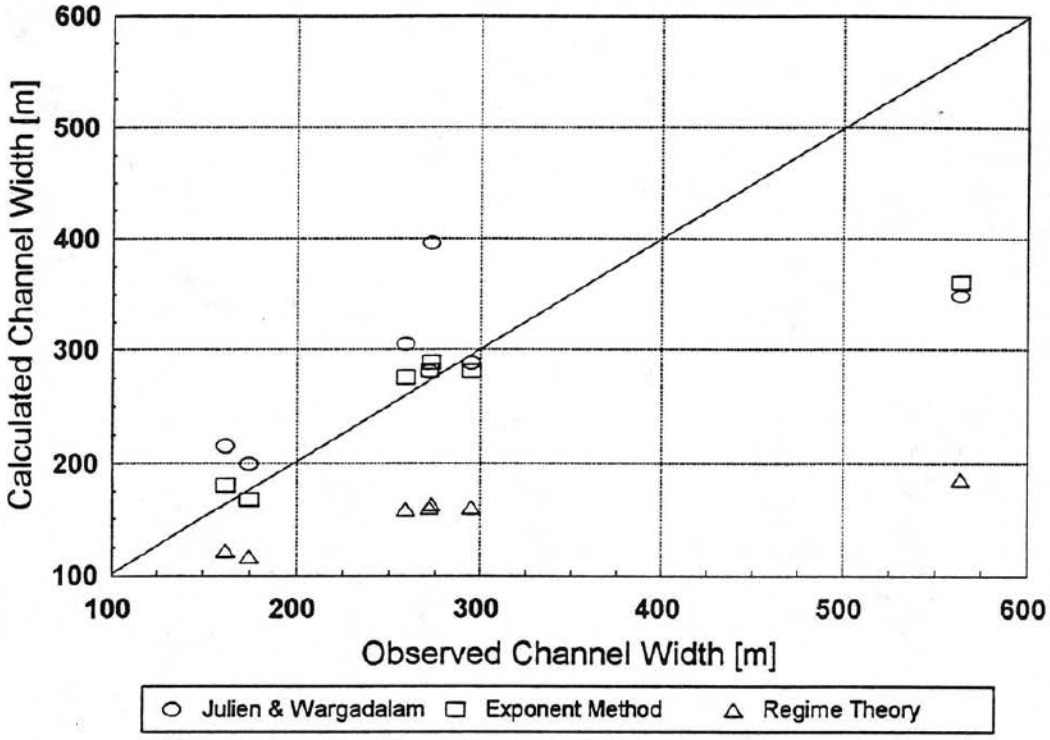

Figure 2. Calculated versus observed channel width at Rio Apure.

Channel depth (Fig. 3) proved to more difficult to predict. Both the regime theory and the exponent methods predicted depths within a very narrow range, and failed to capture the downstream variability in depth. On the other hand, Julien and Wargadalam method overestimated the observed depth consistently by about 2 meters, but modeled the downstream variability in depth more appropriately.

Average velocity in the downstream direction (Fig. 4) was not modeled perfectly by any of the three methods. But, Julien and Wargadalam method was the only one that simulated the decreasing downstream trend in velocity, although it consistently underestimated observed velocities by about 0.2 m/s. Both, the exponent method and regime theory results show an increase in average velocity downstream (this is not clear from the Fig. 4, but the reader is advised to consult the appropriate result tables). Julien and Wargadalam method clearly provides more information on the dynamics that govern the characteristics of alluvial channels, than the other two methods.

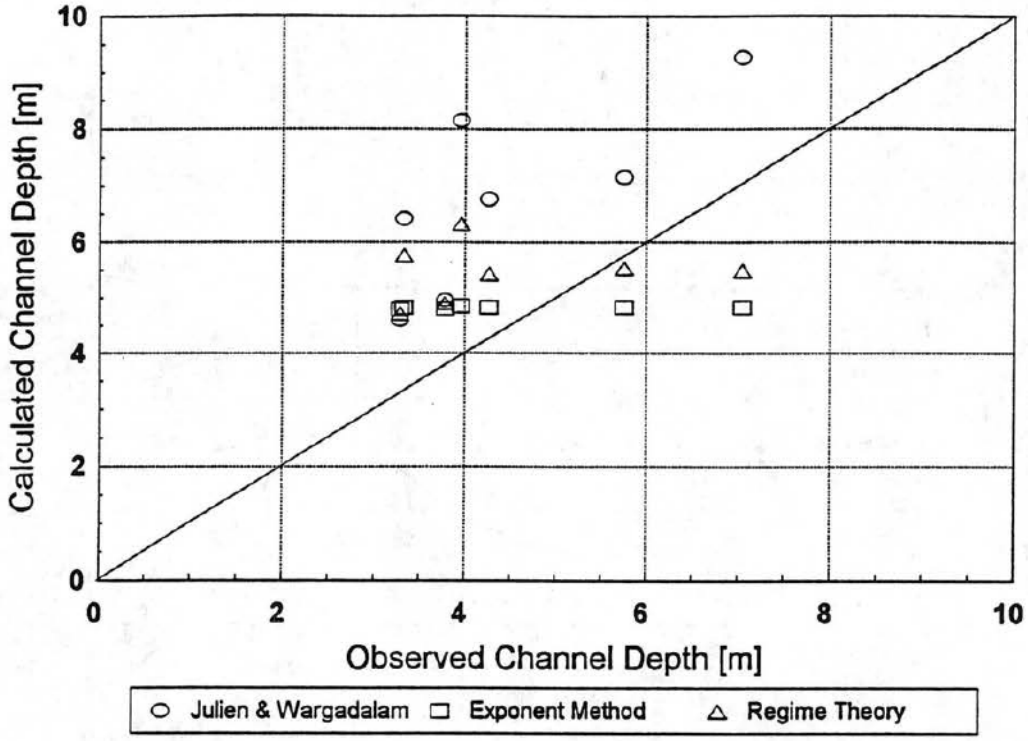

Figure 3. Calculated versus observed channel depth at Rio Apure.

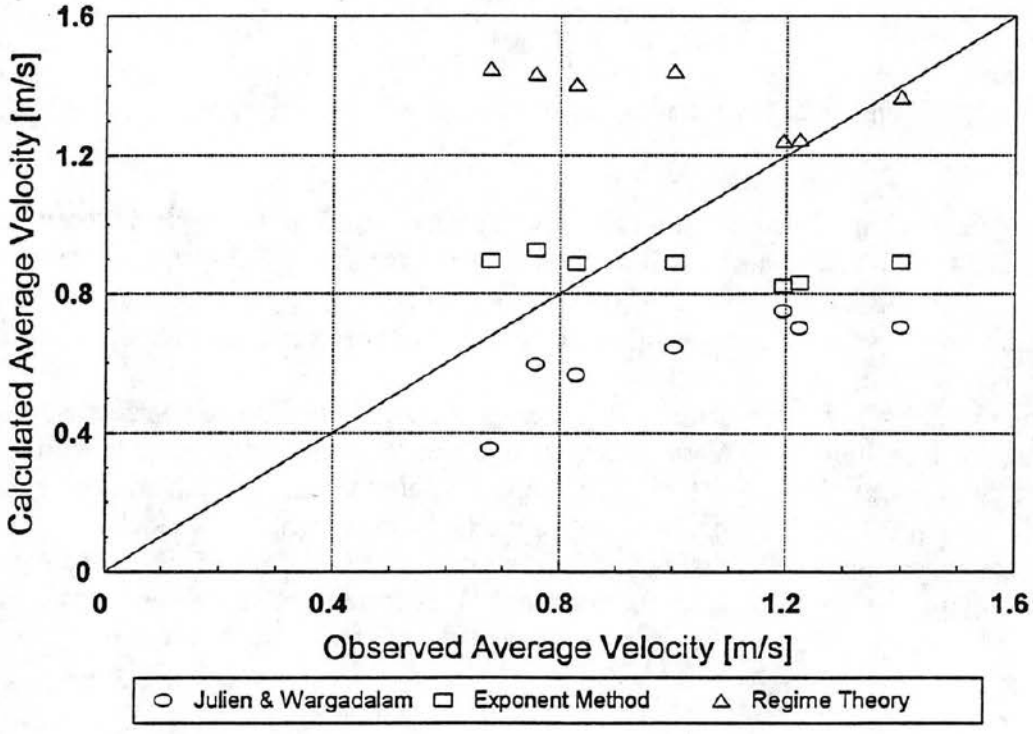

Figure 4. Calculated versus observed average velocity at Rio Apure.

CONCLUSIONS

The results of this exercise can now be summarized. The regime theory predicts channel geometry of stable alluvial channels. Channel slope is considered as a dependent variable in this context, and therefore the results will strictly apply to rivers which have a similar slope as the one computed by the regime theory. The upstream reaches of Rio Apure did not fall into this category. The theory does include a sediment size characteristic in its predictions of stable channel geometry. The regime theory was not calibrated for the conditions of Rio Apure, nor for tropical South American rivers in general. In light of this, the results of this method presented here were surprisingly good.

The exponent method was the only method calibrated for the conditions of the Rio Apure. The fact that its predictions of downstream channel geometry were not always superior to the other two methods is due to the fact that the June 1987 experiment which provided data for this analysis was not an average year. The method depends on discharge as the only driving, independent variable. Its predictions were very good for the downstream variation of width, but lacked in predicting depth and average velocity.

Julien and Wargadalam method is the most sound method from the physical perspective. It includes discharge, slope and sediment size as the independent variables. It was calibrated for a wide range of alluvial rivers, and was the only model in this exercise that predicted the dynamics of the channel geometry appropriately (by dynamics I mean the variability downstream), although consistently underestimating velocity and overestimating depth. The observed decrease in velocity downstream was predicted by this method only.

This study presents one particular condition, for one particular river, and its results should be viewed from that perspective. The variation of hydraulic geometry downstream cannot be exactly predicted and described by any of the above models or methods. And in this sense comparing the methods between each other does not, and can not, lead to any general conclusions on the "quality" of each individual method.

REFERENCES

Julien, P.Y. and Wargadalam, J., 1995. Alluvial channel geometry: Theory and applications. *Journal of Hydraulic Engineering*, 121(4), pp:312-325.

Kolberg, F.J. and Howard, A.D., 1995. Active channel geometry and discharge relations of U.S. Piedmont and Midwest streams: The variable exponent model revisited. *Water Resources Research*, 31(9), pp:2353-2365.

Leopold, L.B. and Maddock, T., 1953. The hydraulic geometry of stream channels and some physiographic implications. US Geological Survey Paper, 252, 57 p.

Rhoads, B.L., 1991. A continuously varying model of downstream hydraulic geometry. *Water Resources Research*, 27(8), pp:1865-1872.

Simons, D.B. and Senturk, F., 1977. Sediment transport technology. Water Resources Publications, Fort Collins, Colorado, 807 p.

Smith, M.E. and Nordin, C.F., 1988. Alignment characteristics of Rio Apure. Basic data report, CER88-89MES-CFN3, Colorado State University, Fort Collins.

Wargadalam, J., 1993. Hydraulic geometry equations of alluvial channels. Ph.D. Dissertation, Colorado State University, Fort Collins, 203 p.

A Method of Riverbank Stability Analysis

By James M. Wilson, M.S. ASME, Ret.

Abstract: An important facet of river morphology and the mechanics of river flow is the lateral movement of the river. For a river to move laterally, the configuration of banks must change. The measure of the bank resistance to lateral change largely lies in its stability. The bank may be viewed as both a conglomeration of soil particles subject to erosion and a structural feature subject to failure. The erosion, whether caused by the river or by lateral flow (groundwater seepage) is the component which changes the structural integrity of the soil embankment. In the past, bank stability has been the purview of geotechnical engineering. However, recently a method of riverbank stability analysis based on geotechnical engineering has been suggested that in-corporates the concepts of river morphology. The primary purpose of the method is to tie erosion to bank stability and predict the degree and rate of bank failure. Inherent in the method is the analysis of bank stability.

Introduction

Although there is a tendency to contemplate river morphology in terms of water flowing down hill, in fact the river as a system can move laterally and even uphill. The system moves by changing the configuration of the banks. Some bank change is due to erosion and deposition of sediment. However, one facet of bank change, while initiated by individual soil particle movement, is in geotechnical terms, a structural failure.

The consequences of bank failure are relatively obvious. Every year thousands of acres of land are lost to encroaching rivers. Individual bank failure has long been studied geotechnically and there are several techniques to predict when a bank or slope will fail. However, until recently there have been few methods available to engineers to properly analyze the dynamics of bank failure in the context of the erosional pressures exerted by the river.

The concept of river morphology often begins with the mechanics of sediment erosion along the stream flow. In fact, the mechanics of river flow including simple hydraulics and sediment transport may be the best understood concepts. However, the dynamics in the transverse direction are less understood or integrated into channel modeling. These include piping/sapping and the lateral drift of the primary channel through bank failure. Although recognized as being inter-dependent, the net simultaneous effect of sediment transport, piping/sapping, and bank failure is complex and difficult to evaluate.

Erosion due to piping/sapping is the result of seepage of water through soil pores and the interstices of rock and is widespread, but not well understood. Hagerty (1991) suggests that the fact that it occurs has not been sufficient to cause consideration of the mechanism as an important erosional process. He further notes that without the conveyance or transport capacity of the river to move sediment presented by the seepage, there would be no head differential and seepage would cease.

However, it is clear that seepage at the toe and face of a riverbank is a factor in sediment transport and the subsequent weakening of the slope from undercutting. The dislodging of sediment is accelerated when the groundwater acts in concert with stream flow. and the principle flow channel is through particles that have less cohesion than the overlying soil horizons. When this occurs, there can be relatively rapid degradation of the toe and bed which serves to widen and deepen the river. The effect carries over into the stability of the bank.

As a bank fails it allows the river to change course. The result affects sediment transport capacity through slope change, velocity vector adjustments and depth changes. The altered flow, in turn, alters the stability of the bank. It is an un-ending cycle. To address this phenomenon, Thorne, et al (1982, 1985, 1988, 1994) developed an integrated system for analyzing and predicting the fluvial erosion and the lateral movement of riverbanks. The method combines erosion theory with geotechnical concepts to permit an estimate of bank stability and the rate of failure. The specific techniques proposed by Thorne for analyzing bank failure are discussed below.

Bank Stability-(Osman-Thorne)

Initial Bank Failure

Osman and Thorne (1985) developed an method of estimating bank stability and bank failure resulting from stream erosion that is based on the geotechnical Mohr-Coulomb failure envelope concept detailed in most geotechnical textbooks similar to Das (1990). The principle is that the

shear stress along a failure plane is related to three soil parameters: c, cohesion of the particles, σ, the average normal stress on a potential failure plane, and ϕ, the internal angle of friction. This can be expressed as a factor of safety, FS:

$$FS = \frac{\tau_r}{\tau_d} = \frac{c_r + \sigma \tan\phi_r}{c_d + \sigma \tan\phi_d} = \frac{\text{average shear strength of the soil}}{\text{average shear stress on the soil}} \quad \text{.....(1)}$$

In other words, if the resistive strength is greater than the applied shear then the soil is stable or if the ratio equals 1, then the slope is at a state of impending failure. c, σ, and ϕ can be determined in the laboratory with relative ease. It can also be said that if

$$FS_c = \frac{c_r}{c_d} \text{ and } FS_\phi = \frac{\tan\phi_r}{\tan\phi_d} \text{ or if } \frac{c_r}{c_d} = \frac{\tan\phi_r}{\tan\phi_d} \text{ then } FS = FS_c = FS_\phi \quad \text{.....(2)}$$

Drawing upon this concept, Osman and Thorne have applied the bank geometry of Fig. 1 and converted Eqn. 1 into a force statement:

$$FS = \frac{\text{Resisting force}}{\text{Driving force}} = \frac{Fr}{Fd} \quad \text{.....(3)}$$

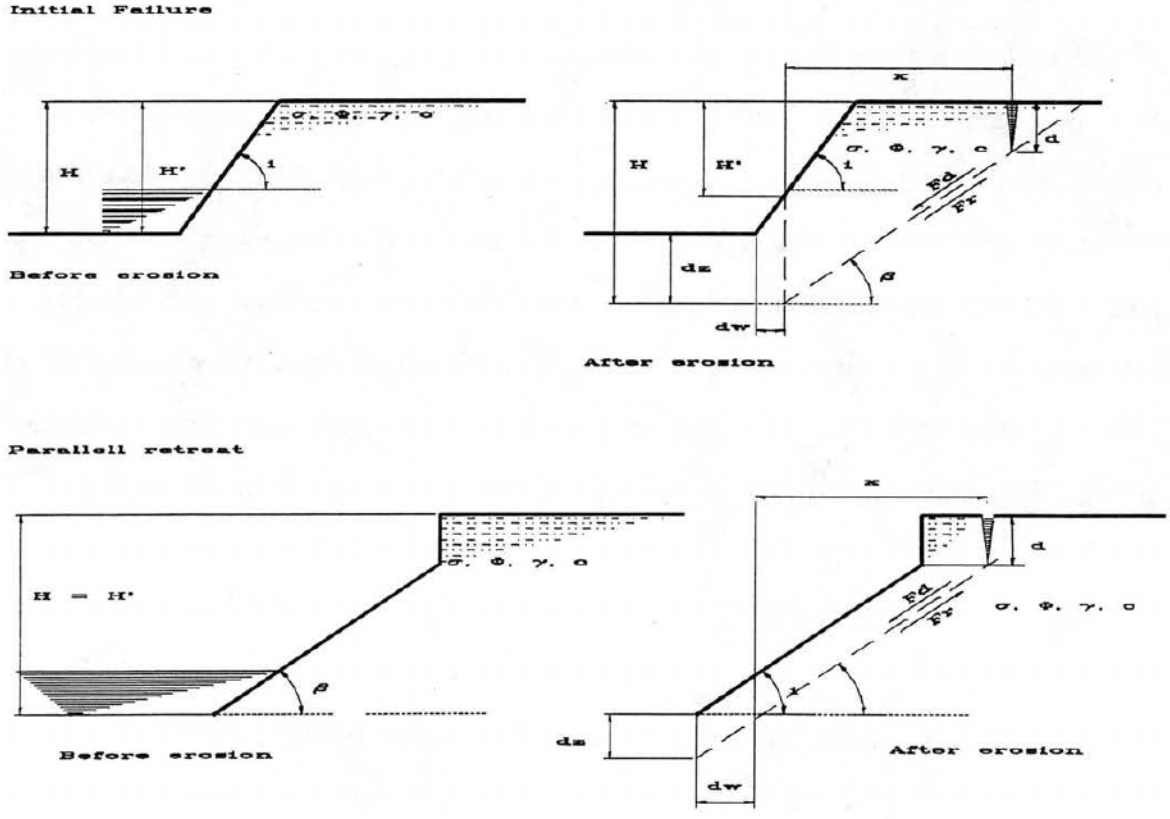

Figure 1. Riverbank erosion and failure sequence

From Fig. 1, it can be seen that when there has been sufficient erosion, the block driven by the weight of the soil mass will slide along the failure plane at angle β,. The erosion is defined by dz and dw.

At this point, it is important to note the assumptions that Osman and Thorne have made in their analysis of the failure of the slab of soil:

- Cohesive, homogeneous soil.
- The failure surface passes through the toe of the bank.
- The effects of vegetation are not considered.
- Water table, seepage, surface runoff, and lateral pressures are not considered.
- Failure surfaces are considered planar, therefore all bank geometry considered in the analysis must a bank angle greater than 60 degrees from the horizontal. Failures below this angle, from a geotechnical standpoint are typically treated as circular.

From geometry, and the properties of the soil, γ, unit weight, and W, total slab weight:

$$F_r = \frac{(H-d)c_r}{\sin\beta} + W_s \cos\beta \tan\phi r \quad \text{.....(3)}$$

$$F_d = W_s \sin\beta \quad \text{.....(4)}$$

$$W_s = \frac{\gamma}{2}\left(\frac{H^2 - d^2}{\tan\beta} - \frac{H'^2}{\tan i}\right) \quad \text{.....(5)}$$

By substitution, Osman and Thorne (1983) found a quadratic solution defined as:

$$\left[\frac{H}{H'}\right]_c = \frac{\lambda_2}{2\lambda_1} + \sqrt{\left(\frac{\lambda_2}{2\lambda_1}\right)^2 - \left(\frac{\lambda_3}{\lambda_1}\right)} \quad \text{.....(6)}$$

where

$$\lambda_1 = \left(1 - \left(\frac{d}{H}\right)^2\right)\left(\sin\beta\cos\beta - \cos^2\beta\tan\phi\right) \quad \text{.....(7)}$$

$$\lambda_2 = 2\left(1 - \left(\frac{d}{H}\right)\right)\frac{c}{\gamma H'} \quad \text{.....(8)}$$

$$\lambda_3 = \frac{\left(\sin\beta\cos\beta\tan\phi - \sin^2\beta\right)}{\tan i} \quad \text{.....(9)}$$

Osman and Thorne presumed that a tension crack would exist in soils with cohesion and defined the depth of those cracks as d. However, if cracks do not exist, then d is simply 0. To evaluate β, the angle of the failure plane, Osman and Thorne turned to earlier works of Taylor (1948) and Spangler and Handy (1973) who suggested that β corresponds to the angle of a plane of fully developed cohesion for which the stability number, $\frac{c}{\gamma H'}$ = maximum.

Therefore, $\frac{d}{d\beta}\left(\frac{c}{\gamma H'}\right) = 0$ and a solution for β can be found:

$$\beta = \frac{1}{2}\left\{\tan^{-1}\left[\left(\frac{H}{H'}\right)^2\left(1-\frac{d}{H}\right)\tan i\right] + \phi\right\} \quad \text{.....(10)}$$

Here again, if no cracks are present, then d = 0.

The initial measured bank and face height can be represented by a ratio and compared to the results of Eqn. 6:

$\frac{[H/H']_c}{[H/H']_m} > 1$ implies stability. $\frac{[H/H']_c}{[H/H']_m} = 1$ implies impending failure. $\frac{[H/H']_c}{[H/H']_m} < 1$ is not possible, therefore the bank has already failed. In practice, it is usual to find that the initial calculation of $\frac{[H/H']_c}{[H/H']_m}$ will be greater than 1.

To find the geometry of the critical case is the goal. To do this, the value of H and H' (measured) must be incrementally changed by dz and dw (Fig. 1) until the measured ratio of H and H' equals the calculated ratio from Eqn. 6. In the process, the value of β must also be re-calculated. When the ratios are equal then the critical geometry is known.

Parallel Retreat

Once initial failure has occurred, the calculated geometry of the slope becomes the starting point for determining the critical geometry of the next failure slab. If the slab failed at a tension crack, then this must be recognized. If not, then d = 0. Recognizing that i now equals β the weight of the block can be defined as:

$$W_s = \frac{\gamma}{2}\left(\frac{H^2 - H'^2}{\tan\beta}\right) \quad (11)$$

and

$$F_d = \frac{\gamma}{2}\left(\frac{H^2 - H'^2}{\tan\beta}\right)\sin\beta \quad (12)$$

Through substitution and solving a quadratic equation:

$$\left[\frac{H}{H'}\right]_c = \frac{\left[\frac{\omega_2}{\omega_1} + \sqrt{\left(\frac{\omega_2}{\omega_1}\right)^2 + 4}\right]}{2} \quad (13)$$

where

$$\omega_1 = \cos\beta\sin\beta - \cos^2\beta\tan\phi \quad (14)$$

and

$$\omega_2 = 2\left(1 - \frac{d}{H}\right)\frac{c}{\gamma H'} \quad (15)$$

As with the initial failure, the value of the "measured" height ratio with respect to the "calculated" ratio must be reiterated until the ratios are equal. This process can be easily accomplished in a computer spreadsheet as demonstrated by Thorne and Abt (1994).

Failure Block Dimensions

Examination and use of the Osman-Thorne method will quickly lead to the realization that the system is extremely sensitive to the location and depth of a tension crack. Darby and Thorne (1994) have addressed this fact and noted that the distance to the crack, x can place the crack

either on the face of the failure block or upon the flood-plane. They have reasoned that a tension crack will develop at the instant of failure and will be at the surface where the block tension just equals the tensile strength of the soil:

$$\sigma_s = \sigma_t \quad \text{.....(16)}$$

where σ_t is defined by:

$$\sigma_t = \frac{ma\sin\beta}{d} \quad \text{.....(17)}$$

and m and a are the mass of the failure block and its acceleration. Darby and Thorne also believe that:

$$a = g(\sin\beta - \cos\beta\mu) \quad \text{.....(18)}$$

and that μ, the coefficient of dynamic friction can be approximated by

$$\mu = \tan\phi \quad \text{.....(19)}$$

By inspection of the geometry and combining Eqns. 10, 16,17,18 and 19, they found implicit equations for the distance to cracks on the riverbank face and on the flood plane:

Cracks located on the bank face:

$$\frac{x^2\tan i}{2} + x(H - H') - \frac{x^2\tan\beta}{2} = \sigma_s \frac{\left[x(\tan i - \tan\beta) + (H - H')\right]}{\gamma\sin\beta(\sin\beta - \cos\beta\tan\phi)} \quad \text{.....(20)}$$

Cracks located on the flood plane:

$$xH - \frac{x^2\tan\beta}{2} - \frac{H'^2 - d^2}{2\tan i} = \frac{\sigma_s(H - x\tan\beta)}{\gamma\sin\beta(\sin\beta - \cos\beta\tan\phi)} \quad \text{.....(21)}$$

In practice, both Eqns. 20 and 21 must be solved. If there is no convergence for a given equation it means there is no crack prediction at that location. If there is no convergence for either equation, there is no crack predicted in any location. However it is possible to have both equations converge. Darby and Thorne have offered no published guidance on how to interpret this result. The authors state that the equations will work both for prediction of initial failure and for subsequent failures provided the proper values are used for variables. For the initial failure H' = H and d = 0. It should be noted that although the presence of the crack can be determined, the

depth for subsequent analysis must be known from on-site observations. Consequently, the Darby and Thorne evaluation of x analytically cannot be divorced from actual field observations. Furthermore, Eqns. 20 and 21 are derived based on some knowledge of the tensile strength of soil in the failure block. This is not easily determined or consistently reliable between block segments of cohesive and/or expansive soils.

Application

The Osman-Thorne method can be demonstrated by a step-by-step caculation of values derived from reasonable, but hypothetical set of conditions:

Initial						
Bank height	Face height	Bank angle	Int. frict.	Cohesion	Unit weight	Crack depth
H	H'	i	ϕ	c	γ	d
m	m	deg.	deg.	Pa	N/m^2	m
3	3	60	7	13,000	17,100	0

Table 1. Bank parameters prior to erosion

Table 1 provides the parameters of an alluvial riverbank of medium sand mixed with clay silt. The unit weight of the soil is for saturation which should produce the worst case condition. If the bed were of the same material and the flow conditions were known, the rate of erosion could be calculated by various means. However, in this example degradation of the channel will not be tied to the river erosion.

Step 1: Using Eqns. 6, 7, 8, 9, and 10, calculate $\frac{[H/H']_c}{[H/H']_m}$

$$\beta = \frac{1}{2}\left\{\tan^{-1}\left[\left(\frac{3}{3}\right)^2\left(1-\frac{0}{3}\right)\tan 60\right]+7\right\} = 33.5 \text{ degrees}$$

$$\text{and } \lambda_1 = \left(1-\left(\frac{0}{3}\right)^2\right)\left(\sin 33.5\cos 33.5 - \cos^2 33.5\tan 7\right) = 0.37$$

$$\lambda_2 = 2\left(1-\left(\frac{0}{3}\right)\right)\frac{13000}{17100 \bullet 3} = 0.51$$

$$\lambda_3 = \frac{\left(\sin 33.5\cos 33.5\tan 7 - \sin^2 33.5\right)}{\tan 60} = -0.14$$

$$\left[\frac{H}{H'}\right]_m = 1 \text{ and } \left[\frac{H}{H'}\right]_c = \frac{0.51}{2 \bullet 0.37} + \sqrt{\left(\frac{0.51}{2 \bullet 0.37}\right)^2 - \left(\frac{-0.14}{0.37}\right)} = 1.61$$

and the stability number, $\frac{[H/H']_c}{[H/H']_m}$ = 1.61. Therefore the bank is stable.

Step 2: Modify the measured dimensions of H and H' by some dz and dw and re-iterate step 1. To simplify the example, only dz is changed. For example, a trial degradation of the bed, dz = 0.5 m means that the new H = 3.5 m. H' remains the same at 3 m. β equals 37 degrees.

$\frac{[H/H']_c}{[H/H']_m}$ = 1.32 The bank is still stable.

By iteration, it can be shown that when the bank becomes critical, dz = 1.56 m, H = 4.56 m, H' = 3 m and β = 41.5 degrees.

Step 3: Assume that subsequent failures will be parallel. Therefore i = β = 41.5 degrees. Again, no crack will be assumed. The initial values of height are: H = 4.56 m and H' = 4.56 m.

From Eqns. 13,14,and 15, the stability number, $\frac{[H/H']_c}{[H/H']_m}$ = 1.46, indicating stability.

Step 4: Again, the depth of channel degradation is modified by iterating dz until the stability number is found to equal 1.

When $\frac{[H/H']_c}{[H/H']_m}$ = 1, dz = 2.11 m, H = 6.68 m, and H' = 4.56 m.

Step 5: Repeat steps 3 and 4. Since the original assumption was that no cracks existed, field observations should be made to test the validity of the assumption. Furthermore, in actual practice it might be wise to produce a sensitivity envelope for each of the original parameters.

Conclusion

Although not discussed above, the ultimate aim of the method after defining the geometry of the failure block is to calculate the volume and apply linear dimensions of bank reach to subsequently derive the rate of failure of the river reach under analysis.

In using the Osman-Thorne, the initial assumptions are important. If the soil is not homogeneous fully saturated, and the bank slope, i greater than 60°, the predictive capability of the equations may deteriorate. In addition, the Darby-Thorne analysis of crack location is extremely restrictive for analytical purposes and probably should only be used where the analyst has good working knowledge of the soils in question. The fact that the equations can be made to converge for two different values of x suggest that while the supporting theory may be valid, ambiguous results may tend to detract from usefulness. At best, the method must be considered as only an estimate. The nature of cohesive soil, consolidation and expansion characteristics, seepage pressures, and the resulting lateral pressures of both soil and the river are not addressed. Nevertheless, the system may provide a useful tool on-site where actual observations can be employed to calibrate the terms.

Appendix I. References

Darby, S. E. and Thorne, C. R. (1994). "Prediction of tension crack location and riverbank erosion hazards along destabilized channels." *Earth Surf. Process. Landforms.* 19(3), 233-245.

Das, B. J., (1990). *Principles of Geo-technical Engineering.* PWS-Kent, Boston, MA.

Hagerty, D. J. (1991). "Piping/Sapping erosion: II. identification and diagnosis." *J. Hydr. Engrg.*, ASCE, 117(8), 1009-1025.

Osman, A. M., and Thorne, C. R. (1988). "Riverbank stability analysis. I: theory and II. applications." *J. Hydr. Engrg.*, ASCE, 114(2), 134-172.

Thorne, C. R., and Abt, S. R. (1994). "Analysis of riverbank instability due to toe scour and lateral erosion." *Earth Surf. Process. Landforms.* 18(9), 835-843.

Appendix II. Notation

a	=	Acceleration of the soil mass.
β	=	Angle of the plane of failure with the horizontal.
c	=	Coefficient of soil cohesion.
d	=	Depth of the tension crack.
dw	=	Horizontal erosion.
dz	=	Vertical erosion.
Fd	=	Driving force along the plane of failure.
Fr	=	Resisting force along the plane of failure.
FS	=	Factor of safety.
ϕ	=	Angle of internal friction.
H	=	Bank height measured from the bed.
H'	=	Bank face measured from the point of erosion.
γ	=	Unit weight of the soil.
i	=	Angle of the bank slope with the horizontal.
λ	=	Coefficient.
m	=	Soil mass.
μ	=	Coefficient of dynamic friction.
σ	=	Normal stress on the plane of failure.
σ_s	=	Tensile strength of the soil.
τ	=	Shear stress along the plane of failure.
ω	=	Coefficient.
x	=	Distance to tension crack measured from the poin of erosion.

LOCAL SCOUR AT BRIDGE PIERS

By Su K Mishra

Abstract: Pier scour has been studied extensively in the laboratories and formulas have been derived by various authors to describe the results of their individual experiments. Although these formulas have been certain similarities, they appear to differ widely. In this paper, some of the existing equations for predicting local scour at bridge piers are compiled. The pier scour data collected at eight bridge sites in the State of Pennsylvania are listed. The pier scour equations obtained at the PSU by performing several regression analyses on the collected data are presented. A comparison of the results from the equations with the measured values of pier scour is made followed by a short discussion and conclusion.

INTRODUCTION

Local scour at bridge piers is a function of bed material size, flow characteristics, fluid properties, and the geometry of the pier. For a number of reasons, many of the researchers have simplified their research by: 1) Assuming that the differences in density, viscosity between laboratory and field conditions can be neglected, 2) Restricting research to steady uniform flow that is unrestricted by bridge structures, 3) Considering only alluvial, non-cohesive, uniform particle-size bed material, 4) Working with single piers that are smooth and aligned with the flow and without scour protection. With these simplifications, the functional form of the equation for the depth of scour, d_s, can be written as:

$$d_s = f(\rho, \nu, d_{50}, \tau, Y_0, U_0, b)$$

where:

ρ = Density of water
ν = Kinematic viscosity of water
D_{50} = Particle size of which 50% of the material is finer
τ = The shear stress
Y_0 = Approach depth of flow
U_0 = Approach velocity of flow
b = Width of pier normal to the flow

Bata (1960)(1), Chitale (1962)(1), Shen et al (1969)(1,5), Shen (1969)(1), Richardson et al (1975)(1), Neill (1969)(1) have predicted different pier scour equations by their individual experiments.

EXISTING PIER SCOUR EQUATIONS:

Each equation will now be presented in its original format followed by a comparison format. Symbols from the following list appear in one or more of the equations:

Y_0 = Approach flow depth
d_s = Scour depth measured from the mean bed elevation
U_0 = Approach flow velocity
D_{50} = Diameter of mean bed material
b = Width of pier

Fr = Froude number of approach flow, $U_0^2/(gY_0)$
F1 = Pier Froude number, $U_0^2/(gb)$

1. Bata (1960) (1)

Original format:

$$\frac{d_s}{Y_0}=10[\frac{U_0^2}{gY_0}-3\frac{d_{50}}{Y_0}]$$

Comparison format:

$$\frac{d_s}{b}=10[(\frac{Y_0}{b})(\frac{U_0^2}{gY_0})-3(\frac{d_{50}}{b})]$$

2. Chitale (1962) (1)

Original format:

$$\frac{d_s}{Y_0}=-5.49Fr^2+6.65Fr-0.51$$

Comparison format:

$$\frac{d_s}{b}=\frac{Y_0}{b}[-5.49Fr^2+6.65Fr-0.51]$$

3. Shen, Schneider, Karaki (1969) (1,5)

Original Format:

$$d_s=0.00073Re^{0.619}$$

where: Re = Pier Reynold's number, U_0b/ν
ν = Kinematic viscosity

Comparison format:

$$\frac{d_s}{b}=4.43Fr^{2/3}(\frac{Y_0}{b})^{1/3}$$

4. Shen (1969) (1)

Original Format:

$$\frac{d_s}{b}=3.4FI^{0.67}$$

Comparison Format:

$$\frac{d_s}{b}=3.4Fr^{0.67}\left(\frac{Y_0}{b}\right)^{0.33}$$

5. CSU equation- Richardson et. al. (1975) (1)

Original Format:

$$\frac{d_s}{Y_0}=2.0K_1K_2\left(\frac{b}{Y_0}\right)^{0.65}Fr^{0.43}$$

where:

K_1 = Pier Shape Coefficient (Discussed later)
K_2 = Coefficient of angle of attack of approach flow (Discussed later)

Comparison format:

$$\frac{d_s}{b}=2.0K_1K_2\left(\frac{Y_0}{b}\right)^{0.35}Fr^{0.43}$$

6. Neill (1964) (1)

Original format:

$$\frac{d_s}{b}=1.5\left(\frac{Y_0}{b}\right)^{0.3}$$

Comparison format:

$$\frac{d_s}{b}=1.5\left(\frac{Y_0}{b}\right)^{0.3}$$

DEVELOPMENT OF NEW PIER SCOUR EQUATIONS AT PSU

A total of eight bridges were considered for the development of an equation for the prediction of the depth of scour at piers. The bridges were chosen with help of the respective Pennsylvania Department of Transportation District offices.

Table 1 lists the parameters that are considered in the study to be relevant in the formation of a predictive equation for scour at piers. The correction coefficient K_1, is adopted from the CSU equation, which is presently endorsed by the Federal Highway Administration in the Hydraulic Circular No. 18 - " Evaluating Scour at Bridges " (4).

Table 1 - Parameter descriptions for development of pier scour equation

Parameter	Description
K_1	Correction coefficient for pier nose shape
θ	Angle of attack
K_2	Correction coefficient for angle of attack
b	Pier width
Y_0	Approach flow depth
U_0	Approach velocity
D_{16}, D_{50}, D_{84}	The respective sediment grain sizes of which X% of the sediment bed is smaller, where X = 16, 50 and 84 respectively

Uniformity coefficient , UC, may be calculated by the following equation:

$$UC = \frac{(D_{84} - D_{50})}{(D_{50} - D_{16})}$$

It is important to note that this is not the same uniformity coefficient that is often used in soil mechanics.

The geometric standard deviation, G is calculated as follows:

$$G = \sqrt{\frac{D_{84}}{D_{16}}}$$

Table 2 shows the values of K_1 for various pier shapes. Table 3 illustrates the values of K_2 for various angles and pier length (PL) to pier width (b) ratios.

Table 2 - Correction factor, K_1, for pier nose shape used by Richardson (4)

Shape of pier nose	K_1 value
Square nose	1.1
Round nose	1.0
Circular cylinder	1.0
Sharp nose	0.9
Group of cylinders	1.0

Table 3 - Correction factor, K_2, for angle of attack of flow used by Richardson (4)

Angle of attack	PL/b = 4	PL/b = 8	PL/b = 12
90	1.0	1.0	1.0
75	1.5	2.0	2.5
60	2.0	2.5	3.5
45	2.3	3.3	4.3
0	2.5	3.9	5.0

REGRESSION ANALYSES:

Case 1:

The first regression analysis was performed using the identical parameters as those used by Richardson (4) in the development of his equations with the addition of the uniformity coefficient (UC), previously described. Table 4 illustrates the hydraulic parameters used in the regression analysis.

The final equation named as PSU1 obtained after performing regression analysis is as follows:

$$\frac{d_s}{Y_0}=0.12K_1\left[\frac{\theta}{90}\right]^{0.015}\left[\frac{b}{Y_0}\right]^{-0.34}(Fr)^{0.157}(UC)^{0.214}$$

Case2:

The regression analysis was again performed, however; the parameter related to the sediment grain sizes was slightly altered. The regression was done using the geometric standard deviation, G, of the grain size distribution in place of the uniformity coefficient (UC). The values of G for all the eight bridges are given in table 5.

Table 4 - Hydraulic parameters used in the regression analysis

Bridge No.	d_s (ft)	Y_0 (ft)	d_s/Y_0	K_1	θ/90	b	Fr	UC
1	2.5	8.38	0.29	1.0	0.833	4.0	0.74	2.1
2	4.0	16.8	0.23	1.1	1.0	6.0	0.48	4.5
3	5.0	13.1	0.38	1.0	1.0	3.0	0.57	5.1
4	2.5	13.8	0.18	1.0	0.722	3.5	0.56	5.43
5	2.5	16.5	0.15	0.9	1.0	7.0	0.28	2.2
6	3.0	16.3	0.18	1.1	1.0	6.0	0.83	2.75
7	2.0	10.8	0.19	1.0	0.5	3.5	0.30	2.75
8	1.0	10.7	0.09	1.1	1.0	7.0	0.52	2.75

Table 5 - Geometric standard deviation values

Bridge No.	G
1	7.8
2	4.32
3	5.4
4	8.73
5	10.75
6	6.1
7	6.1
8	6.1

The equation after performing the regression analysis named as PSU2 is given by:

$$\frac{d_s}{Y_0} = 0.31 K_1 \left(\frac{\theta}{90}\right)^{0.148} \left(\frac{b}{Y_0}\right)^{-0.52} Fr^{0.061} G^{-0.47}$$

Case3:

The regression analysis was performed on the parameters, as in the other cases with the difference that, the correction coefficient for angle of attack, K_2, developed by CSU and used in the CSU pier scour equation was adopted in place of the parameter (θ/90). Also, the uniformity coefficient (UC) previously defined was used as a parameter. Table 6 gives the K_2 values for all the eight bridges.

Table 6 - Values of correction factor K_2, for the bridges

Bridge No.	K_2
1	2.375
2	1.0
3	1.0
4	3.3
5	1.0
6	1.0
7	4.0
8	1.0

The final equation named as PSU3 after regression analysis, is found to be:

$$\frac{d_s}{Y_0}=0.13K_1K_2(\frac{b}{Y_0})^{0.216}(Fr)^{0.4}(UC)^{0.336}$$

Case 4:

The regression analysis of case 3 was repeated using the geometric standard deviation, G, in stead of the uniformity coefficient, UC. The equation after performing regression analysis named as PSU4 was determined to be :

$$\frac{d_s}{Y_0}=0.45K_1K_2(\frac{b}{Y_0})^{-0.48}(Fr)^{0.1}(G)^{-0.45}$$

COMPARISON OF RESULTS

Table 7 is a compilation of the computed scour depth to pier width ratios, as computed by the equations discussed previously. Actual measured scour depth to pier width ratios are given at the bottom of the table. Figure 1 also illustrates the computed scour depth to pier width ratios versus the actual measured values.

The equations developed for the pier scour did not produce a consistent scour prediction for the bridges studied. The regression analysis for each case had a very low R^2 value. This comparison also indicates that the CSU equation which is presently endorsed by the FHWA is unable to predict the extent of pier scour correctly, thus indicating the need for an improved predictive equation.

Table 7 - Comparison of scour depth to pier width ratios

Equation	Bridge 1	Bridge 2	Bridge 3	Bridge 4	Bridge 5	Bridge 6	Bridge 7	Bridge 8
Bata	11.1	2.4	10.5	12.2	1.7	18.5	2.4	3.9
Chitale	2.9	1.5	4.9	5.9	2.2	3.3	3.05	2.24
Shen et al	4.63	2.75	4.5	4.7	2.5	5.4	2.9	3.3
Shen	3.6	2.11	3.5	3.6	1.9	4.2	2.2	2.5
CSU	4.7	1.63	2.6	7.7	2.4	2.9	1.0	1.9
Neill	1.3	1.1	1.5	1.6	1.4	1.4	1.5	1.2
PSU1	0.36	0.17	1.12	1.0	0.33	0.61	0.55	0.26
PSU2	0.35	0.16	1.27	0.83	0.31	0.66	0.63	0.27
PSU3	0.63	0.18	0.57	1.74	0.18	0.41	1.1	0.22
PSU4	1.24	0.26	1.77	4.0	0.44	0.59	3.77	0.39
Actual	0.63	0.25	1.67	0.71	0.36	0.5	0.57	0.14

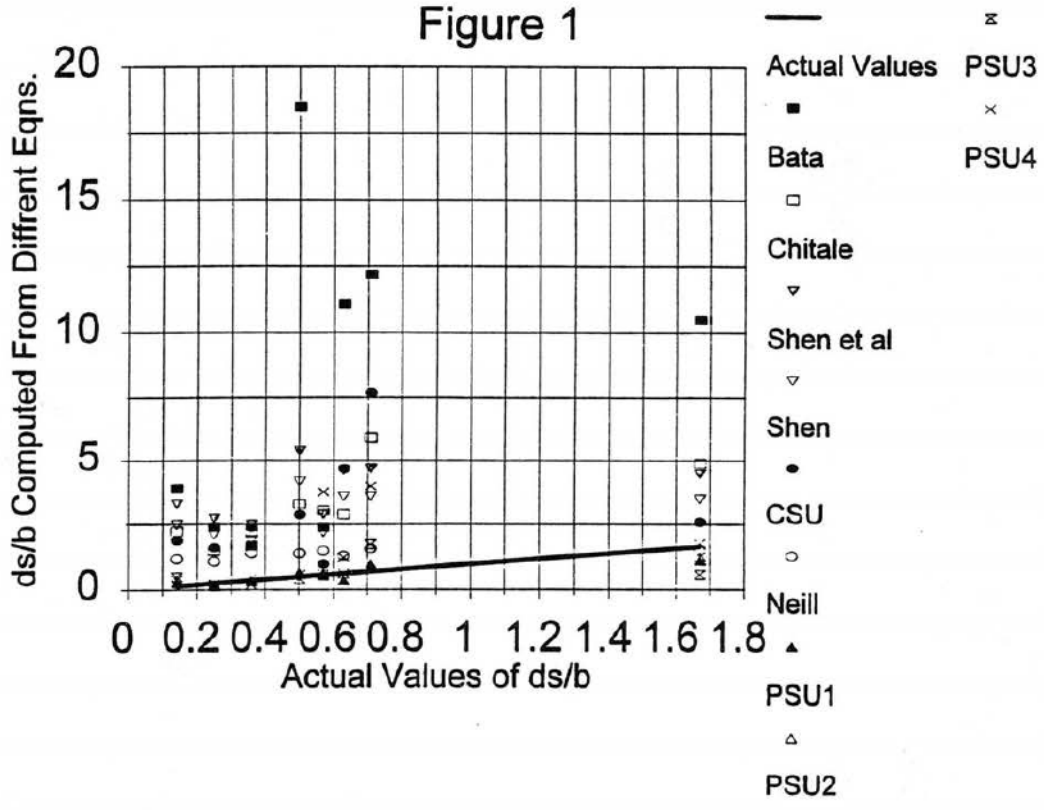

DISCUSSION AND CONCLUSION

The most significant conclusion of the study is the inappropriateness of applying the existing equations to the streams in Pennsylvania. The existing equations currently used and recommended by various sources over predicted the actual measured scour at the study sites. The economic impact of using the existing equations is unmeasurable. Estimates from a number of practicing engineers and professionals indicated that thousands of dollars per bridge could be saved in drilling and excavation costs associated with placing the footers at extreme depth, thus indicating the need for an improved predictive equation for pier scour.

REFERENCES

1. Miller, A.C., Johnson D., Steinhart, R. (1992). "Bridge scour prediction methods applicable to streams in Pennsylvania." *Prepared for Pennsylvania Department of Transportation, Research Project No. 89-03.*
2. Raudkivi, A.J. (1986). "Functional trends of scour at bridge piers." *ASCE Journal of Hydraulic Engineering, Vol. 112, No. 1.*
3. Richardson, E.V. and Richardson, J.R. (1989). "Bridge Scour." *Bridge scour symposium, Cosponsored by FHWA and USGS, October 17-19.*
4. Richardson, E.V., Harrison, L.J., and Davis, S.R. (1991). "Evaluating scour at bridges." *Sponsored by FHWA, Publication No. FHWA-IP-90-017.*
5. Shen, H.W., Schneider, V.R., and Karaki, S. (1969). "Local scour around bridge piers." *ASCE Journal of Hydraulic Division, Vol. 95, HY6.*

FLUID MUD IN NAVIGATION CHANNELS

by Maria Cueto

ABSTRACT

The equations which govern the rheological properties of fluid mud, the effect of fluid mud on ship motion, and dynamics of fluid mud motion are reviewed. The model considered was a two-layer fluid, an upper layer of fluid with a newtonian behavior and the lower layer with non-newtonian rheology. The characteristics of the fluid mud in the entrance channel on Orinoco River are presented. The values for the initial rigidity and viscosity, using the Granboulan et al. and Marccuci models are estimated.

INTRODUCTION

An important problem in river engineering is the deposition of fine sediment in navigation channels located at the downstream area of the rivers. Dredged navigation channels in coastal areas are effective sediment traps where the increased water depth increase rates of sedimentation by reducing bottom stresses induced by waves and currents. During major storms and other extreme events, suspended sediments are well mixed throughout the water column, but as the energy levels decline, they settle gradually to form dense layers of fluid mud near the bottom.

The objective of this paper, which is based on a thorough literature review is to provide a description of the theoretical foundation of fluid mud behavior, an analysis of the sediment characteristics and their influence in ship motion, also a case study will be presented.

Fluid mud may be defined as a cohesive mixture of clay- and silt sized sediment in the flocculated state. It may also contain organic matter and, at times, smalls amounts of very fine sand (Mehta and Maa, 1986).

The study of fluid mud behavior in navigation channels is very important because there are two elements of concern related to it:

- The complex problem of handling this type of sediment, which generates problems in the maintenance of the navigation channel itself, and
- Effect of fluid mud in the motion of ships traveling along the channel.

PROPERTIES OF FLUID MUD

Shear Stress

The steady state shear stress induced in a fine cohesive sediment is commonly believed to result from friction due to the relative motion and interaction of fluid and the sediment particles in

a time invariant flow. Jenkins and Aijaz, 1994, indicate the formation process of the layer of sediment: Unlike coarse sediments, the fine sediments do not behave as individual units but are bound together as flocs. Flocculation takes place when sediment-laden freshwater mixes with seawater containing salts. In freshwater where there are no ionic solutions, the fine silt and clay particles carry a large electric double layer compared to their radii. The electric double layer constitutes the charge of the particles and equivalent amount of counterinos. As the freshwater mixes with seawater, the cations in the salt are attracted toward the surface of the particle. Some of these neutralize the charge on the particle, resulting in compression of the double layer. The compaction of the double layer causes the electric potential at the shearing plane between the solid-liquid interface to drop rapidly. The repulsive forces become small and the particles can approach each other to form flocs. Jenkins and Aijaz, 1994, conducted experiments and showed that the variations of shear stress in fluid mud are related to electrokinetic properties associated with the charged particles that make up the flocs. They observed that the shear stress increased exponentially with increasing sediment concentration. The shear stress increased logarithmically with increasing salinity. The growth of shear stress was rapid in the lower-salinity range (0-3 ppt), while the increase was gradual in the higher-salinity range (3-30 ppt).

Rheology

Foda, et al.,1993, present the equations which govern the rheological behavior of fluid mud. The shear strain γ is sinusoidal in time t with frequency ω:

$$\gamma = |\gamma| e^{-i\omega t} \qquad (1)$$

The resultant shear stress $\tau(t)$ is nearly sinusoidal but with a phase shift σ.

$$\tau = |\tau| e^{-I(\omega t+\sigma)} \qquad (2)$$

This phase shift implies that the material has a complex shear modulus G, since

$$G = \tau/\gamma = G^o e^{-i\sigma} \quad G^o = |\tau/\gamma| \qquad (3a)$$

$$G = G' - iG'' = G^o(\cos\sigma - i\sin\sigma) \qquad (3b)$$

The real part of G, G', represents the elastic shear storage modulus, and the imaginary part, -G", represents the viscous shear loss modulus. For a zero phase shift, $\sigma = 0$, the shear loss modulus is zero and the response is purely elastic, while a phase shift of $\pi/2$ indicates completely viscous response. Equivalently, the material may be described by a complex kinematic viscosity ν defined by

$$\nu = \tau/(\rho\gamma) = (G'' + iG')/\rho\omega \qquad (4)$$

A real ν means a viscous response, an imaginary ν means an elastic response, and a general complex ν characterizes a viscoelastic response. By measuring $|\tau|$, G' and G" can be obtained from equation (3b) . Three empirical regimes are proposed to describe the behavior of the sediments:

Elastic: At strain amplitudes less than some critical strain amplitude γ_e, the cohesive sediment can be completely described as an elastic solid of storage modulus $G' = G_e$ and loss modulus $G'' = 0$.

Viscoelastic: For intermediate strain amplitudes the cohesive sediment displays viscous and elastic behavior, i.e., nonzero G' and G". The strain amplitude in this regime is bounded by two critical values: a lower limit of the elastic yield, γ_e, and an upper limit of the viscous critical strain, γ_v.

Viscous: At the highest strain amplitudes the sediment is modeled as a purely viscous fluid. This occurs when the phase shift equals 90°, $|\gamma| > \gamma_v$.

EFFECT OF FLUID MUD IN SHIP MOTION.

One of the important physical aspects of the problem of fluid mud in navigation channels, concerns the influence of the underlaying movable silt-covered bottom, this influences the maneuvering characteristics of the vessel. The effect of the underlaying viscoelastic mud layer is most pronounced when the clearance between the ship bottom and the top of the mud layer (interface) is relatively small.

D'Ambrosio and Molero, 1987, mention the effects produced to the ships traveling through navigation channels with muddy bottoms:

- Increased resistance, causing the operator to increase the RPM'S to assure constant velocity as well as diminishing sensibly the stopping distance.

- Diminishing ship's forward course as well as reducing turning velocities.

- Reduction on rudder's efficiency for a given propeller angular velocity, causing a large turning radius.

According to Miloh, 1995, there is strong indication that the proximity of the ship bottom to the mud layer may have a pronounced effect on both its propulsion and maneuvering characteristics. He indicates that the occurrence of variations of temperature, combined with possible vertical gradients of salt content, introduce regions of considerable density changes (pynocline) separating two well-mixed layers of uniform density. When vessels traveling in channels which present these highly stratified characteristics, frequently suffer a sudden loose of their speed and steering capabilities. In order to illustrate the influence of the viscosity on the wave resistance in a channel, Miloh defines the wave resistance coefficient as a function of the wave resistance, Rw of a moving pressure patch in a finite-depth channel with a viscoelastic muddy bottom. The pressure p_o, is applied over a rectangular region, L = length, B = width. The wave resistance coefficient is expressed as:

$$C_w = \frac{1}{2} \frac{\rho g L}{p_o} \frac{R_w}{B L p_o} \qquad (5)$$

Miloh, plotted it versus the inverse-square Froude-number:

$$\frac{1}{2F^2} = \frac{gL}{2U^2} \qquad (6)$$

Figure 1 demonstrates the influence of mud viscosity and mud density on the wave resistance

for the case of dimensionless water depth d/L = 0.2 and mud depth d'/L = 0.1. From figure 1a can be seen that when the mud viscosity is very low it is the case of water with total depth d/L = 0.3. A dimensionless viscosity $\nu'/(gL^3)^{1/2} = 1$ is seen to represent a very rigid mud layer. From Figure 1b can be noticed that for very dense mud the shallow case of d/L = 0.2 is approached.

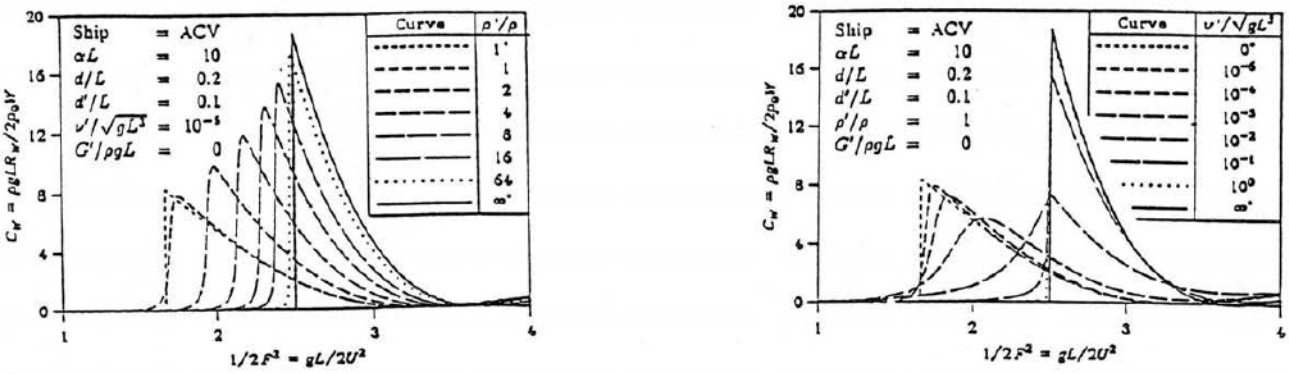

Figure 1: a) Effect of mud viscosity. b) Effect of mud density (from Miloh, 1995).

DYNAMICS OF MUD MOTION

Mehta and Maa, 1986, present an analysis of the characteristics of soft mud response under progressive, non-breaking waves, particularly with respect to erosion. Mehta and Maa, schematized the relationships among the various physical process, Figure 2 presents the sketch:

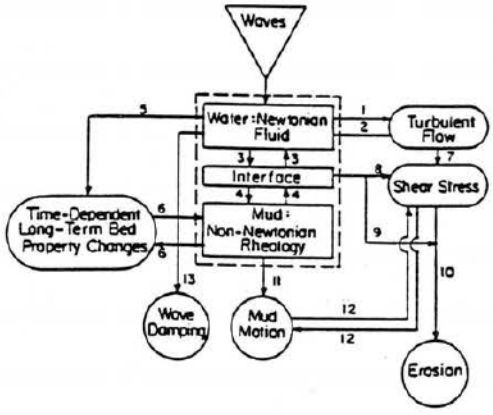

Fig. 2: Schematic description of Wave-Mud dynamics (from Mehta and Maa, 1986)

In this figure, the box with dashed line represents the two-layered mud/water system, rectangles within the box are components of the two-layered system, inverted triangle is the wave forcing function, ovals are process transfer function and circles the results.

Mehta and Maa, 1986, developed a multi-layered hydrodynamic model for evaluating particle velocities in water and mud layers, the corresponding dynamic pressure and shear stress profiles and,

from the latter, the interfacial bed shear stress, τ_b. In addition, the model gives the surface wave attenuation coefficient. Figure 3 is a definition sketch for the layered water-mud system.

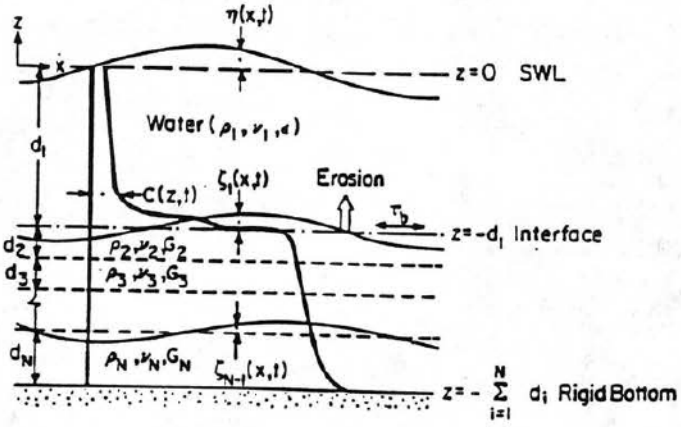

Fig 3: Definition sketch for the Water-Mud System (from Mehta and Maa, 1986)

The free displacement, η, and mud layer displacement ζ_i are given by

$$\eta(x,t) = ae^{i(kx-\sigma t)} \qquad (7)$$

$$\zeta(x,t) = b_i e^{i(kx-\sigma t)} \qquad (8)$$

where

a = water wave amplitude
b_i = unknown complex variable specifying mud sublayer amplitude (and phase)
k = complex water wave number
σ = frequency
$j = (-1)^{1/2}$, the real part of k is $2\pi/L$
L = wave length

The imaginary part of k (=D) represents the attenuation coefficient for the amplitudes a and b_i in the x-direction. D is defined by: $a_x = a_0 \exp(-Dx)$, where a_0 is the initial (x=0) wave amplitude, a_x is amplitude at a distance x. The linearized forms of the equations of motion for an incompressible flow, with a viscous upper fluid (water) and viscoelastic lower (mud) layers are:

$$\frac{\partial u_i}{\partial t} = -\frac{1}{\rho_i}\frac{\partial p_i}{\partial z} + \nu_{ei}\left(\frac{\partial^2 u_i}{\partial x^2} + \frac{\partial^2 u_i}{\partial z^2}\right) \qquad (9)$$

$$\frac{\partial w_i}{\partial t} = -\frac{1}{\rho_i}\frac{\partial p_i}{\partial z} + \nu_{ei}\left(\frac{\partial^2 w_i}{\partial x^2} + \frac{\partial^2 w_i}{\partial z^2}\right) \qquad (10)$$

where u_i, w_i are the horizontal (x-direction) and vertical (z-direction) velocity components, I=1 for water, 2 for mud and

$$\upsilon_{ei} = \upsilon_1 + \varepsilon, \qquad for\ i = 1$$

$$\upsilon_{ei} = \upsilon_i + \frac{jG_i}{\rho_i \sigma}, \qquad i = 2 \ldots, N$$

The physical significance of linearization is that the equations are applicable to conditions involving small amplitude waves and small shear strains in the mud. The form of the complex viscosity term in Equation 4 for mud arises out of the assumption of a Voigt solid representation of viscoelastic material under an oscillatory load. The pressure, p_i, in Equations 9 and 10 is given by

$$p_i = p_i^t + \rho_i g z + p_i^o \qquad (11)$$

where p_i^t = total pressure and

$$p_i^o = 0 \qquad for\ i = 1$$

$$p_i^o = [\sum_{i=1}^{N-1} (\rho_i \ \rho_{i-1})]\ g(\sum_{i=2}^{N-1} d_i) \qquad for\ i=2 \ldots . , N-1$$

The continuity equation for each layer is

$$\frac{\partial u_i}{\partial x} + \frac{\partial w_i}{\partial x} = 0 \qquad (12)$$

The solutions for variables u_i, w_i, and p_i are assumed to be

$$u_i(x,z,t) = \hat{u}_i(z) e^{j(kx-\sigma t)} \qquad (13)$$

where $u_i\hat{}$, $w_i\hat{}$, $p_i\hat{}$ are the corresponding amplitudes.

$$w_i(x,z,t) = \hat{w_i}(z)e^{j(kx-\sigma t)} \qquad (14)$$

$$p_i(x,z,t) = \nu_{ei}\left(\frac{\partial u_i}{\partial z} + \frac{\partial w_i}{\partial x}\right) = \hat{\tau_i}(z)e^{j(kx-\sigma t)} \qquad (15)$$

Orinoco River

The Orinoco River has a total length of 2100 km, its drainage area covers 950,000 Km^2. The delta of the river, with an area of about 30,000 Km^2, begins about 190 Km from the Atlantic. The Orinoco is navigable for oceangoing ships for some 360 Km from the mouth to the city of Puerto Ordaz. The channel is a deep-draft navigation waterway which permits the navigation of vessels with dead weight tonnage (DWT.) up to 80,000 and drafts from 9.8 m in low water up to 12.8 m during high water. The average river flow rate is around 30,000 m^3/s. The tidal range in the entrance channel area is 0.3 m during neap tides and 2.1 m during spring tides (registered in the gage station at 24.9 River Kilometer).

The presence of fluid mud in the Navigation channel of Orinoco River has been reported in the entrance channel, specifically, between 0 RK (river kilometer) to 77.7 RK, between the 55.5 and 77.7 RK,(see appendix), the presence of fluid mud depends on the daily tidal variations and seasonal variations of the saline wedge. In the external channel, the lithology is represented by fine sand, clay and silt; in some cases horizontal stratifications of sand and clay can be found distributed in a regular pattern. In this section of the channel occurs a complex sedimentation mechanism due to: sediments transported by the river, sediment transport due to swell and currents along the seacoast, recirculation of dredged material, the sediments trap created by the navigation channel itself and the presence of the saline wedge. The distribution of the sediments along the external channel is presented in Table No. 1.

Table No. 1: Type of sediment along External Channel of Orinoco River. (CAURA, 1994)

River Kilometer	Sediments
0.0 - 55.5	Silt, clay and some calcareous material
55.5 - 66.6	fine sand, silt and clay
66.6 - 77.7	sand and silt

The conjunction of the action of the tide and the river flow leads to the formation of a large mass of fine sediment in suspension, the thickness of the layer can achieves up to 2 m and can be found along the external channel (Romero and Soto, 1993). The concentration of material in suspension vary from 0.03 - 1.16 g/l near the surface, but can achieves values up to 141 g/l close to the bed Lira, 1995; for semiconsolidaded mud the concentration can be up to 300 g/l. The settlement of suspended matter takes place during the neap tide slack water periods and leads to heavy sedimentation. Such siltation generates problems in the calculation of the dredged volume and to the vessels traveling through the navigation channel because sediment can accumulate in the form of layers of fluid mud with concentrations greater than 300 g/l. The presence of fluid mud can be detected by using an echosounder, but this technique does not permits to know the vertical variations in the density , figure 4 presents an extract from an echosounder recording at the RK 13.0 at the entrance channel in Orinoco River.

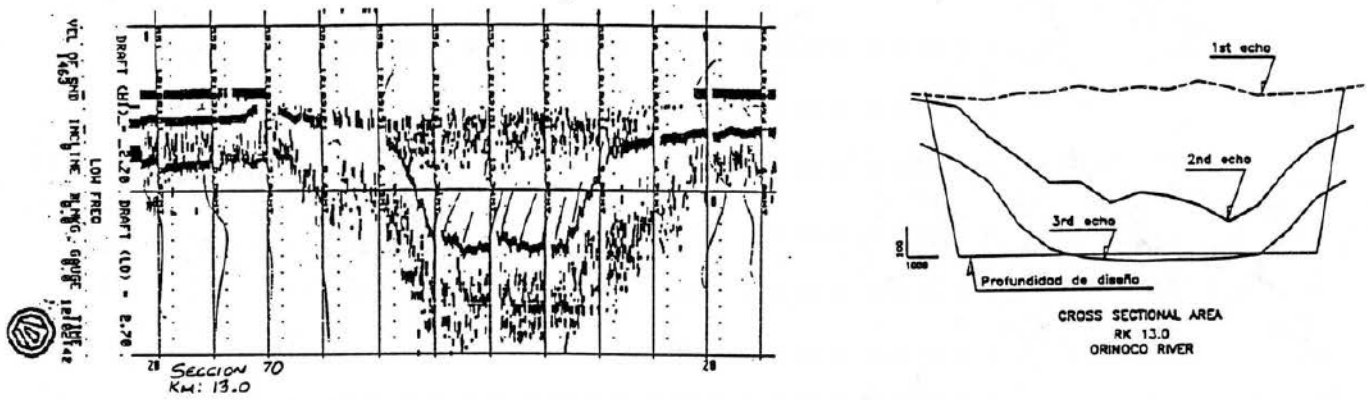

Figure 4: Extract from an echosounder recording of the channel in Orinoco River Entrance (Echotrack).

The different situations which can be generated in the interpretation of the echosounder recording, are presented by D'Ambrosio and Molero, 1987 :

- The appearance of a strong return over the echo instrument printed register is correlated with a change in the existing acoustic impedance over the material that is subject to the reflection. Suspension's reflections with high sediment concentration occurs due to its density vertical gradient distribution in such a way that the layers producing reflections are not associated to a particular density value but to zones of rapid changes in density. This means that the instrument sends an acoustic echo which is returned at the moment it touches a particular strata plotting its position on the echograph. This strata consist on layer in which there is a rapid change in density and every time the echo finds similar situations it will register this information on the recording causing multiple registrations at different depths. This causes enormous complications to define the true bottom of the channel.

- Another situation is generated where there is a sufficient high value of fluid mud density in such a way that the reflections occurs at the borderline between water and fluid mud and this situation

is positioned at a level close to the hard bottom in such a way that the first reflection causes confusion with respect to the record registered by the second reflection emitted through the echosounder transducer given by the hard bottom. However , in this particular case the depth interpretation is easy to determine but it is needed to draw its outline in a conservative way in the water-fluid mud interface considering nevertheless, that the real depth is higher than the given value.

- Another case that have to be considered is when exists an appreciable fluid mud variable thickness, with an irregular shape, showing variable intensities in which is recognized fluid mud-water interface as well as the hard bottom. In this particular case, it is not possible to determine with confidence a nautical depth. It depends more on the interpretation and technical experience of the analyst-surveyor on the office.

All the above elements have to be considered when vessels report that there are not sufficient depth in the navigation channel and when the estimation of dredging quantities is made by using the hydrographic surveys of pre and post dredging.

Lira, 1995, presents the results of analysis of samples taken at different points along the entrance channel of Orinoco River. The salinity analysis was made using an YSI instrument, model 33. The determination of suspended solids and dissolved solids was made by using the gravimetric method. Figure 5 presents the results of the analysis in the form of contour diagrams for the salinity, density, suspended solid and dissolved solids along the entrance channel.

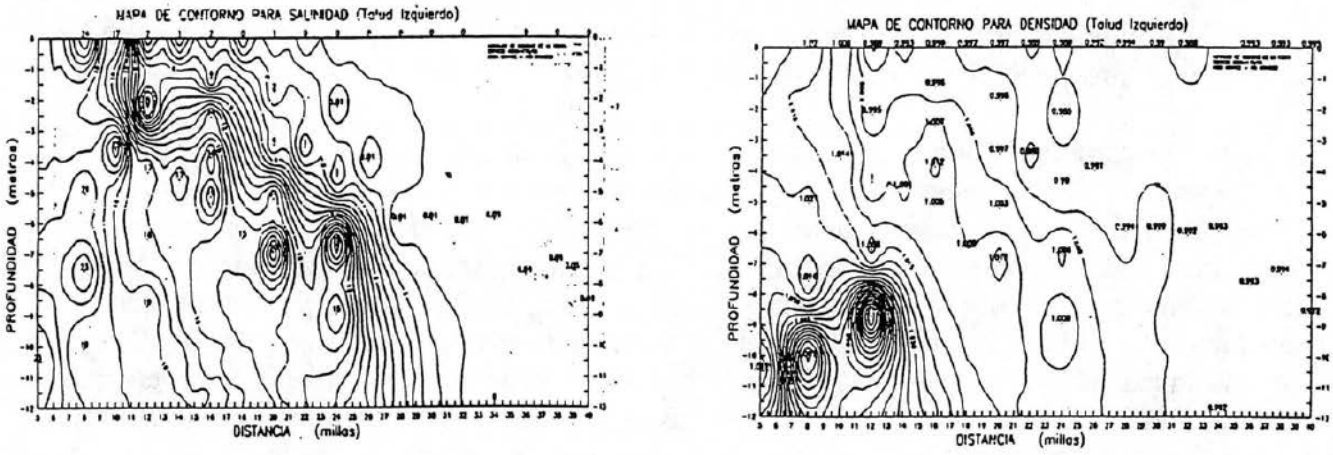

Figure 5a: Contour diagrams for the salinity, density, suspended solid and dissolved solids along the entrance channel in Orinoco River (from Lira, 1995)

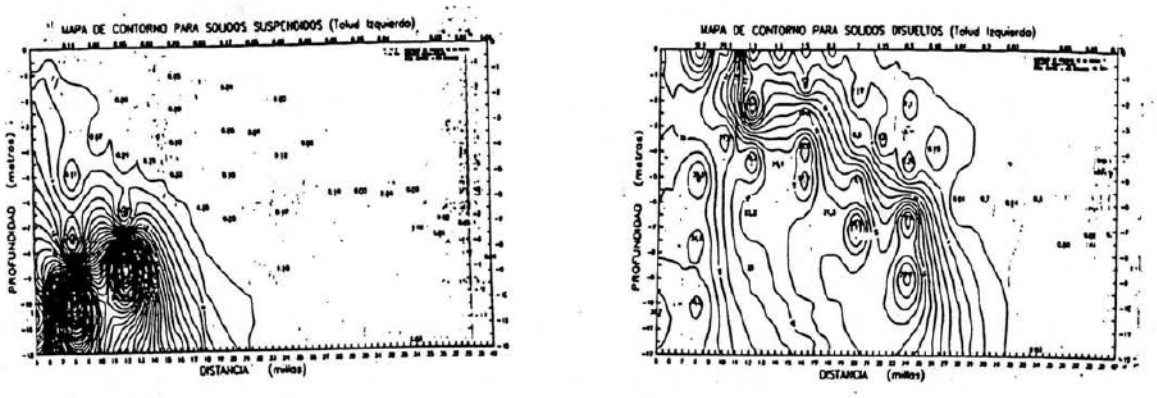

Figure 5b: Contour diagrams for the salinity, density, suspended solid and dissolved solids along the entrance channel in Orinoco River (from Lira, 1995)

The equations given by Granboulan et al., 1989, were used in order to evaluate the magnitude of the rheological properties of the fluid mud in Orinoco River, it is important to notice that these equations were obtained for the Gironde River (France). The initial rigidity and the viscosity are:

$$\tau_y = e^{(\frac{C}{79} - \frac{318}{79})}$$

$$\eta = 2.45x10^{-6}\ C^{1.857}$$

where τ_y = initial rigidity(Pa); C = solid mass concentration (g/liter); η = dynamic viscosity (Poise).

The equations given by Marcucci, 1994, which were derived for fluid mud in equatorial regions, were used in order to compare with that obtained for the Gironde River:

$$\tau_y = 2.75x10^{-7}C^3$$

$$\eta = 1.76x10^{-14}C^6$$

Table No. 2 and figure No. 6 present the results, as can be noticed, the values for initial rigidity obtained with the equations given by Marcucci, are higher than those obtained with the Granboulan, et al. formulation; the higher difference is in the order of 0.66 Pa. In the case of dynamic viscosity, there are more agreement among the values, the higher difference is 0.11 Poises. It is important to notice that these equations were derived for different conditions to the Orinoco River. For the values of dynamic viscosity obtained, the mixture display properties of Bingham bodies.

Table 2: Relation between concentration and dynamic viscosity and initial rigidity in Orinoco River at the entrance channel.

RK	Sal (‰)	C (g/l)	ρ(g/l)	τ(Pa)	η(Poise)
14.8	19	94.5	1.092	0.059	0.011
22.2	15	141	1.146	0.106	0.024
24.0	19	80.8	1.112	0.050	0.0085
29.6	15	106	1.084	0.068	0.014
44.4	19	112	1.114	0.074	0.016

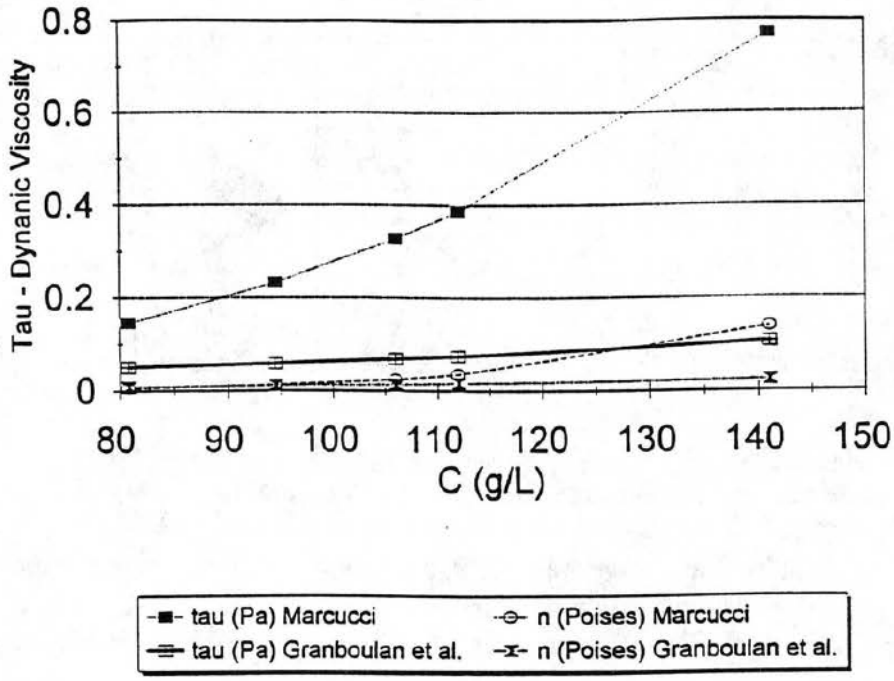

Figure 6: Relation between concentration and dynamic viscosity and initial rigidity in Orinoco River at the entrance channel

CONCLUSIONS.

The area of the entrance channel of Orinoco River is influenced by the combination of the tidal action and the sediment flow from the river, which leads to the formation of the large mass of fine sediments in suspension. The navigation channel is influenced by these movements and the channel by itself is a sediment trap. The progress of a vessel which has to navigate through the entrance channel is hindered by the rheological state (rigidity and viscosity) of the fluid mud environment. The correlations between concentration and dynamic viscosity and rigidity have to be determined for the specific characteristics of the Orinoco River, then, it is required a systematic sampling and measurement plan, in order to obtain these parameters.

REFERENCES.

- Aijaz, S. And Jenkins, S. (1994) "On the electrokinetic of shear stress behavior in fluid-mud suspensions". *Journal of Geophysical Research*. Vol. 99, No. C6, pp 12697-12706

- CAURA. (1994) "Estudio de Impacto Ambiental producido por el dragado de mantenimiento en el Canal del Orinoco" Caracas, Venezuela.

- D'Ambrosio, C. And Molero, A. (1987) "Reporte sobre el fenómeno del fluff". Instituto Nacional de Canalizaciones. Caracas, Venezuela.

- Foda, M., Hunt, J. And Chou, H. (1993) "A nonlinear model for the fluidization of marine mud by waves". *Journal of Geophysical Research*. Vol. 98, No. C4, pp 7039-7047.

- Granboulan, J., Feral, A. and Villerot, M. (1989) "Study of the sedimentological and rheological properties of fluid mud in the fluvio-estuarine system of the Gironde Estuary". *Ocean & Shoreline Management*, Vol. 12, pp 23-46.

- Marcucci, E. (1994) "Estudio del fluff del canal exterior de Maracaibo". INCOSTAS. Caracas, Venezuela.

- Mehta, A. And Maa, P. (1986). "Waves over mud: modeling erosion". In *Third International Symposium on River Sedimentation*. The University of Mississippi, Jackson.

- Miloh, T. (1995) "Ship Motion in Non-Homogeneous Media". *Ship Technology Research*. Vol. 42, pp 140-156.

- Lira, A. (1995) "Determinación de la salinidad, sólidos disueltos, sólidos suspendidos y densidad en muestras de agua- Desembocadura del Rio Orinoco". Universidad Central de Venezuela. Caracas, Venezuela.

- Romero, R. And Soto, R.(1993) "Comportamiento del Fluff en los Canales de Navegación y su Influencia en la Navegación" In *I Seminario Seguridad en los Canales de Navegación*. Caracas, Venezuela.

APPENDIX: Navigational Entrance Channel - Orinoco River.